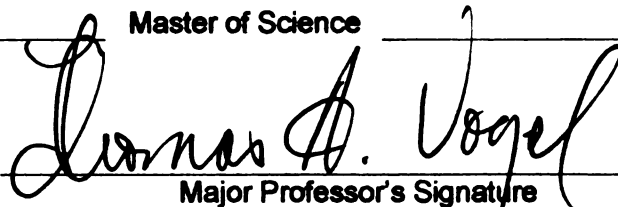This is to certify that the
thesis entitled

The Origin of Silicic Domes in the Vicinity of the Makiling
Stratovolcano in the Macolod Corridor, Philippines: Evidence
From Bulk Chemistry, Mineralogy and Oxygen Isotopes

presented by

Melissa Sue Wilmot

has been accepted towards fulfillment
of the requirements for the

Master of Science

Major Professor's Signature

3/22/05

Date

PLACE IN RETURN BOX to remove this checkout from your record.
TO AVOID FINES return on or before date due.
MAY BE RECALLED with earlier due date if requested.

DATE DUE	DATE DUE	DATE DUE

THE ORIGIN OF SILICIC DOMES IN THE VICINITY OF THE MAKILING
STRATOVOLCANO IN THE MACOLOD CORRIDOR, LUZON, PHILIPPINES:
EVIDENCE FROM BULK CHEMISTRY, MINERALOGY AND OXYGEN
ISOTOPES

By

Melissa Sue Wilmot

A THESIS

Submitted to
Michigan State University
in partial fulfillment of the requirements
for the degree of

MASTER OF SCIENCE

Department of Geological Sciences

2005

ABSTRACT

THE ORIGIN OF SILICIC DOMES IN THE VICINITY OF THE MAKILING STRATOVOLCANO IN THE MACOLOD CORRIDOR, LUZON, PHILIPPINES: EVIDENCE FROM BULK CHEMISTRY, MINERALOGY AND OXYGEN ISOTOPES

By

Melissa Sue Wilmot

The origin of high-silica magmas in areas lacking continental crust is not well-understood. The Macolod Corridor on Luzon Island of the Philippines provides an ideal area to study to this problem. Two end-member models, partial melting of previously emplaced magma batches and fractional crystallization, have been developed to explain the formation of high-silica magmas. The silicic domes (Bulalo, Bijang, Olila and Calamba) examined in this study are located near the Makiling Stratovolcano. The mineralogy and chemical composition of Bulalo, Bijang and Olila are very similar, while Calamba shows some slight differences. Most of the evidence developed in this study supports partial melting of discrete batches of previously emplaced crystallized magma as the likely source for the high-silica magmas composing the domes. The composition of domes can only be produced through the partial melting of an andesitic/dacitic source. The Sr concentration in the domes is too high to indicate the fractionation of large amounts of plagioclase. Neither the An content of plagioclase phenocrysts nor the Sr/Ba ratio indicates that fractional crystallization could have produced the chemistry of the domes. The observed difference in REE patterns of Calamba may be due to a larger degree of partial melting. The oxygen isotope values are similar for the three domes analyzed, indicating a similar source for the dome magmas. The high-silica Mt. Makiling samples most likely originated from a different source magma than the dome samples.

ACKNOWLEDGMENTS

TABLE OF CONTENTS

LIST OF TABLES

Images in this thesis are presented in color.

INTRODUCTION

Silicic volcanic rocks are abundant in continental arcs, but not widely recognized in oceanic arcs. It has only recently been recognized that silicic rocks can be found in abundance in areas lacking continental crust. Areas such as the Kermadec Arc (Smith et al., 2003a, Smith et al., 2003b) and the Izu-Bonin Arc (Tamura and Tatsumi, 2002) are currently being studied. The silicic domes in the vicinity of the Makiling Stratovolcano in the Macolod Corridor on Luzon Island of the Philippines, are another example and provide an ideal setting to investigate how silicic magmas form in oceanic arcs. The composition and origin of these domes are the focus of this study.

The study of the formation of high-silica magmas is important for many reasons. Understanding the evolution of high-silica magmas in oceanic arcs may provide insight into how continental crust evolved. Also, high-silica magmas often erupt with highly explosive force due to the high viscosity and gas-content of these magmas. Because many people live in close proximity to areas actively erupting high-silica magmas, an understanding of how they form may provide insight into how to predict the eruptions.

There are two end-member models that have been used to explain the evolution of high-silica magmas in areas lacking continental crust: fractional crystallization of mantle derived magmas, and partial melting of previously emplaced magma (Riley et al., 2001; Tamura and Tatsumi, 2002; Singer et al., 1992; Brophy and Dreher, 2000). In one model of fractional crystallization, a magma evolves through the crystallization of early formed minerals, either by side-wall crystallization or crystal settling. This allows for a more siliceous melt to form. This process is considered to be unrealistic by some workers due to the large amount of fractionation needed. A variation of the crystal fractionation

model involves the formation of a partially-solidified layer that advances downward through the chamber (Brophy and Dreher, 2000). In this model, the fractionated liquid is trapped in this layer until it has crystallized enough to become rigid. At this point, the layer may fracture, allowing the more evolved liquid trapped between the crystals to become segregated from the other components. This becomes the more evolved liquid that eventually may erupt at the surface or stall in the crust (Brophy and Dreher, 2000).

Partial melting is the other end-member model. In arc regions, recent workers have suggested that an influx of magma may cause partial melting of plutons of varying compositions (e.g. Tamura and Tatsumi, 2002; Tamura et al., 2003; Riley et al., 2001). Early work focused on the formation of high-silica magma through the partial melting of basaltic and andesitic rocks. Beard and Lofgren (1991) performed several melting experiments in which they began with rocks of those compositions and melted them in anhydrous and hydrous conditions at different pressures. They were able to produce melts of granodioritic and trondhjemitic composition. Based on the Beard and Lofgren (1991) experiments, Tamura and Tatsumi (2002) suggested that hydrous calc-alkaline andesites emplaced in the crust were the source of the rhyolites of the Izu-Bonin arc. In Tamura and Tatsumi's (2002) model, the magmas crystallize and stall before they reach the surface because high water content decreased the liquidus temperature. An influx of hot, basaltic magma reheats and partially melts these calc-alkaline andesites, remobilizing them and erupting rhyolitic lava on the surface.

The purpose of this paper is to determine the processes that led to the formation of four of the domes located near the Makiling stratovolcano. The main question to be addressed is: How did the high-silica magma form? A second question is: How are the

2

four domes related to one another and to the Makiling stratovolcano? Data used in this study include: petrographic analysis, bulk chemsitry, mineral phase and glass composition, and oxygen isotope values of the whole rock and individual minerals.

GEOLOGIC SETTING

The Philippine Archipelago is located in an oceanic arc that also contains ophiolite and continental terranes (figure 1), although these compose only a small part of the islands as part of the Palawan Terrane (figure 2) (Knittel et al., 1988). The Philippine archipelago lies south of Taiwan, between the South China Sea to the west and the Philippine Sea to the east. This area is geologically complex because it is situated between two opposing subduction zones involving the Eurasian Plate and the Philippine Sea Plate, in an area of intense deformation (Cardwell et al., 1980). The Philippine Trench and East Luzon Trough occur off the east coast of Luzon, the northernmost and largest island in the Philippines. These formed due to the westward subduction of the Philippine Sea Plate. The Manila, Negros and Cotabato Trenches occur off the west coast, and formed due to the eastward subduction of the Eurasian Plate (Bautista et al., 2001). A series of N-S trending faults formed as a result of the compressional and shearing forces caused by the opposing subduction zones. The longest area of faulting is the Philippine Fault Zone, which extends from Mindanao in the southern Philippines to northern Luzon (Bautista et al., 2001).

The subduction zone located off the east coast of Luzon has been the cause of Late Miocene to Recent volcanic eruptions (Mukasa et al., 1987). The subduction at the East Luzon Trough is not currently related to active volcanism, most likely due to the shallow angle of subduction (Defant et al., 1989). In contrast, the western coast of Luzon is the site of active subduction-related volcanism, which formed the "Luzon arc" that extends from Taiwan to Mindoro. The Luzon arc is divided into five segments based on a

difference in tectonic settings and magma evolution processes: Mindoro, Bataan, N. Luzon, Babayan and Taiwan (Defant et al., 1989).

The silicic domes examined in this study occur near the Makiling Volcano in the Macolod Corridor, which is an extensional zone between the Mindoro and Bataan segments of the Luzon Arc (figure 2) (Sudo et al., 2001). The Macolod Corridor stretches 60 km across Central Luzon, an area which contains no continental terranes (Defant et al., 1989). The Macolod Corridor consists of a basement composed of intrusive bodies and limestone. The oldest rocks in this area include a sequence of Paleocene-Oligocene San Juan metavolcanics and metasediments, and early to mid-Miocene San Juan quartz diorite (Sudo et al., 2001; Oles, 1991). The initiation of the most recent episodes of volcanism in the Macolod Corridor is not well-constrained, with estimates ranging from 1.8 to 0.6 Ma. Volcanism continues through the present (Defant et al., 1989; Sudo et al., 2001). The formation of the Corridor is still a matter of debate, although the general consensus is that it is a pull-apart rift zone (Bautista et al., 2001; Mukasa et al., 1994; Sudo et al., 2001). This may have led to the extensive faulting that is observed in the Corridor. Bulalo Dome alone is surrounded by several normal faults (Aquino, 2004).

Many types of volcanic activity have occurred in the Corridor. Other volcanic deposits in this area include basaltic scoria cones and maars, active solfatara fields (fumarole-type structures characterized by sulfurous emissions (Bates and Jackson, 1957)) ash-flow tuffs, and stratovolcanoes (Forster et al., 1990, Sudo et al., 2001). Two large calderas occur in the Corridor: Laguna de Bay and Taal Volcano (Figure 3). The youngest silicic samples from Laguna de Bay have been dated at 42-47 ka and 27-29 ka

(Catane and Arpa, 1998). Mount Taal has been active as recently as 1969, although this eruption was mostly basaltic in character (Sudo et al., 2001). The three stratovolcanoes that occur in the Corridor are Mt. Banahaw, Mt. Makiling, and Mt. Malipunyo. A series of monogenetic volcanoes that erupt basaltic magma are also located here. These monogenetic volcanoes include 42 scoria cones and 36 maars that have been dated at 1.05 ± 0.05 Ma and 0.84 ± 0.13 Ma (Sudo et al., 2001).

Several domes are found in the area between Laguna de Bay and Taal Lake (figure 4). The domes to be investigated in this study are all located near Mt. Makiling, a large stratovolcano composed of andesitic and dacitic lava flows, airfall deposits and pyroclastic flows (Sudo et al., 2001). No data on the age of the volcanic deposits of Makiling are available. The domes in this area include Mt. Bijang, Calamba (Mt. Mapinggoy), Olila, Bulalo, and Trapiche (Tanuaun Hill) (figure 4), none of which have been previously studied. Ar/Ar dating performed on Trapiche, Bulalo and Bijang yielded ages of 43±17 ka, 15±7 ka and 66±14 ka respectively (table 1) (Heizler, personal communication, 2003).

DATA COLLECTION AND ANALYSIS

Data Collection

Of the many obsidian domes present throughout the Macolod Corridor (Sudo et al., 2001), many of them are not accessible. The six domes that were sampled had been exposed in areas such as road cuts and quarries, making sample collection possible. Four of these domes (Bulalo, Olila, Bijang and Calamba) were chosen as the focus of this study because they had been recently exposed by construction projects, providing easy access to fresh samples. Also, the domes chosen cover a wide area and contain abundant mafic enclaves.

Data were collected from samples from each of the four domes by several methods. Bulk chemical analysis of both major and trace elements was carried out using X-Ray Fluorescence (XRF) and Laser Ablation Inductively Coupled Plasma Mass Spectrometry (LA-ICP-MS) at Michigan State University. Individual mineral phenocrysts and matrix glass were analyzed for major and trace elemental compositions using the Electron Microprobe Analyzer (EMPA) at the University of Michigan. LA-ICP-MS was used as well. Oxygen isotope data for minerals from Calamba, Bulalo and Bijang were collected using the CO_2 laser fluorination/mass spectrometer at the University of Wisconsin-Madison.

Bulk chemical analysis was performed on glass disks composed of fused samples. The disks were prepared following the procedure outlined in Hannah et al. (2002) and Viray (2003). Where possible, the host rocks were separated from the enclaves during the sample preparation process. Enclaves that were large enough were analyzed separately from the host samples.

Minerals and glass from the matrix were analyzed for major elements and some trace elements using EMPA. Mineral phases analyzed included plagioclase, hornblende, pyroxene, magnetite and ilmenite. For these phases, analyses were done one point at a time using a Cameca SX 100 EMPA. It was equipped with five wavelength spectrometers using an accelerating potential of 15 kV. Other settings, including beam spot size, counting time, and beam strength varied based on the phase being analyzed. Glass from the host matrix and the enclaves was also analyzed using EMPA. Analyses of glass in the matrix were carried out using two different methods. If there were an area in which a section of glass was free of microlites, one or two points were taken in that area. This was commonly used in the enclaves because there were clear areas of glass between the needle-like plagioclase grains and phenocrysts. In the host samples, a 5-μm beam was used, and points were analyzed at 15-μm increments. Areas of 3 points by 4 points, or 45μm by 60μm were analyzed in this way. A lower beam strength was used to analyze the glass as well. Both of these analytical methods limited the migration of volatile elements such as Na, and improved the results of the analyses. The compositions of each point were then examined, bad totals eliminated, and the rest averaged to obtain the glass compositions.

Trace elements were collected from plagioclase and hornblende using LA-ICP-MS. Data were collected from selected plagioclase grains that had been analyzed using the microprobe. The same points were analyzed using a glass standard (NIST 612) and the Ca concentrations collected from EMPA as an internal standard. The laser was focused to a 25 μm sampling size and penetrated the sample at a rate of 3 μm/sec. The peak intensities of ^{88}Sr, ^{138}Ba and ^{44}Ca were collected.

Oxygen isotope values were obtained using CO_2 laser fluorination/mass spectrometry. The procedure followed in order to prepare the dome samples for oxygen isotope analysis was carried out with an emphasis on collecting zircons. Zircons are the preferred mineral for analysis because they record the initial values for a magma and are resistant to reset by subsequent processes. Sample preparation began with the crushing of large amounts of sample. Approximately 25 pounds of sample from each of three domes was crushed and ground in the same method as for the bulk chemical analysis. Such large amounts were needed in order to collect enough zircons for analysis, and a sufficient amount of sample was only available for Calamba, Bijang and Bulalo. The second step was mineral separation, with an emphasis on separating out zircons. The crushed sample was separated by the following method: First, the sample was shaken down a gold table to separate the light from the heavy minerals. Once the mineral separates were dry, a hand magnet was used to separate out the magnetic minerals in preparation for the next step, separation using a Franz Isodynamic Magnetic Separator. The samples were separated further using methylene iodide. Methylene iodide contains a known density in which zircons were expected to sink while the less dense minerals would float, allowing for the separation of zircons from the rest of the minerals. Finally, the grains were separated out by hand using a microscope and tweezers. Because zircons were not found in a large enough abundance to analyze, hornblende, feldspar and magnetite were separated out for oxygen isotope analysis.

Petrographic Analysis

The mineral assemblages of each dome are very similar, with Bijang, Bulalo and Olila containing an almost identical mineral assemblage, and the Calamba samples containing a slightly different assemblage (for a complete description of the mineralogy of each dome, see Appendix 1). The samples from Olila, Bulalo and Bijang are porphyritic. Phenocrysts compose 15-25% of the samples. The matrix is glassy and microlitic. Mafic enclaves of varying sizes are found in Olila and Bulalo. None were observed in the Bijang samples. Plagioclase composes up to 70% of the phenocrysts in each of the domes (figure 5). Generally, the grains are euhedral, with sizes that range from 0.2 to 2.5 mm, and are equally distributed. Plagioclase grains with a sieve texture and/or deep embayments (figure 5b) are rare in all three domes, as are grains with a sieve-textured core and well-zoned rim (figure 5c). Most of the plagioclase grains also contain slight embayments and rounded edges, possibly indicative of slight disequilibrium. A few of the grains contain well-defined outer rims, although these are more common in the enclaves (figure 5d). A glomerophyric texture is common in all three domes, with many of the larger plagioclase grains found in clusters (figure 6a). Occasionally these clusters also contain other minerals, including hornblende, opaques, and, rarely, pyroxene. These clusters may represent pieces of wall-rock that were taken up during the eruption and are not part of the host magma.

The other minerals found in Bulalo, Olila and Bijang include hornblende, opaques and orthopyroxene, in order of abundance. Hornblende (figure 7a) composes 25-30% of the phenocrysts. The hornblende grains are mostly euhedral, with sizes that range from 0.2 to 0.7 mm. The grains also contain slight embayments and rounded edges, with rare

sieve textures. The opaque grains (figure 7b) observed in the domes are magnetite. No ilmenite was analyzed in these three domes. Magnetite composes ~5% of the phenocryst assemblage of the domes. These grains are generally subhedral to anhedral. The larger opaque grains are around 0.7 mm, although most of the grains are much smaller. The opaques rarely contain embayments. Orthopyroxene (figure 7c) is the least abundant mineral in the three domes, composing less than 5% of the assemblage. Only Bulalo contains more orthopyroxene than opaques, although the difference is very small. The pyroxenes are generally euhedral, with sizes as large as 0.7 mm. However, most are significantly smaller, with an average size of 0.1 mm. The larger grains typically show signs of resorption, while the smaller grains typically do not.

The Calamba samples are petrographically different than the other three domes. The matrix of most of the Calamba samples is devitrified, contrary to the other domes. Only one sample (020517-2d) contains a glassy matrix. The major petrographic difference between Calamba and the other three domes is that amphibole is only a minor mineral phase, composing <1% of the assemblage. Instead, pyroxene is the second most abundant mineral phase, composing 25% of the phenocryst assemblage. Also different than the other three domes is the presence of both clinopyroxene (figure 7d) and orthopyroxene. Exact proportions can not be estimated due to the difficulty distinguishing the two types visually, however. The pyroxenes are generally larger than those found in the other three domes, with sizes ranging from 0.05 to 0.23 mm. The third most abundant phase is the opaques, and both magnetite and ilmentite are present in the Calamba samples, in contrast to the other three domes. The textures of the minerals from Calamba generally are similar to the other domes.

Mafic enclaves are present in Olila, Calamba and Bulalo (figure 8). The enclaves observed in Olila and Bulalo vary in size. The major differences between the large and small enclaves are the size of the grains and the textural evidence of interaction with the host magma (see appendix 1 for an in-depth description of the enclaves). The enclaves from all three domes are composed mostly of plagioclase. The matrix is composed of needle-like plagioclase grains of varying size. The needle-like grains rarely contain a compositional rim or sieve-textures. Larger phenocrysts of plagioclase are also present in the enclaves, although they are rare. These grains occasionally contain sieve textures and deep embayments. The next most abundant phase in Bulalo and Olila is hornblende, constituting 45% of the phenocrysts. Generally, the hornblende are anhedral and fill the space between the plagioclase grains. However, some euhedral hornblende grains are also present. Pyroxene is a rare phase in the enclaves of Olila and Bulalo. Both hornblende and pyroxene are common phases in the Calamba enclaves. It is often difficult to distinguish them visually because they fill the spaces between the plagioclase grains, not allowing the use of cleavage planes or shapes to distinguish them visually. Euhedral grains of pyroxene and hornblende are also present in the enclaves of Calamba, although the type of pyroxenes present is unknown. Opaque grains occur in the enclaves of all three domes.

Bulk Chemical Composition

Major elements

The Bulalo, Bijang and Olila domes have similar host compositions, whereas the host composition of Calamba is distinctly different. The Calamba dome is dacitic (64-66% SiO_2); whereas Bulalo, Bijang and Olila are dacitic to rhyolitic (69-73% SiO_2)

(figure 9). Calamba also contains higher concentrations of Al_2O_3, Fe_2O_3, MgO, and CaO (figure 10). The mafic enclaves from Calamba, Olila and Bulalo are similar in composition (figure 10), with a silica content of 50-55% (figure 9).

Trace elements

There is some variation in the trace element concentrations between Calamba and the other three domes (figure 11). The concentration of Sr and Rb in the four domes is very similar, while Calamba contains a much higher concentration of Y and Sm than the other three domes. Calamba is also more enriched in the middle rare earth elements (MREEs) compared to the other domes. The chondrite normalized rare earth element (REE) pattern for all of the domes is a concave upward trend. This trend is more pronounced in Bulalo, Bijang and Olila than it is in Calamba (figure 12a). The difference is also observed in a plot of Dy/Lu versus La/Lu (figure 12b), in which Dy represents the MREEs. Olila, Bulalo and Bijang all have values between 0.6 and 0.87, falling below the values of Calamba, 0.85 – 1.05. The MREEs are strongly partitioned into amphiboles, with partition coefficients ranging from ~3 to ~13 (Rollinson, 1993). Therefore, depletion in MREEs is commonly attributed to the presence of amphibole in the source of a magma. Y and Sm are also strongly partitioned into amphibole. The enclaves do not show the depletion in MREEs, with Dy/Lu ratios greater than 1.0. Calamba contains a higher concentration of the light rare earth elements (LREEs) (figure 12b) as well, with La representing the LREEs on the diagram. None of the domes show a negative Eu anomaly (figure 13). Sr has a high partition coefficient into plagioclase, and is concentrated between 200-400 ppm in the host dome samples (figure 11).

Mineral Chemistry

Individual mineral phenocrysts were analyzed using EMPA. Grains analyzed included plagioclase, hornblende, orthopyroxene, clinopyroxene, magnetite and ilmenite. Points were taken in the center and edge of the plagioclase, as well as the area in-between, where noted. If the plagioclase grain was small, points were labeled with numbers, with the first point analyzed in the center of the grain and the second point analyzed near the edge of the grain. For all other mineral types, two points were analyzed, typically one point near the center of the grain and one point near the edge of the grain.

Plagioclase

The general trend for the host plagioclase grains is a decrease in anorthite (An) content from center to edge. There were slight differences among the compositions of the plagioclase grains from each dome despite this general trend. The An content of the center of the plagioclase grains differed slightly between the domes, as did the composition at the edge of the grains. The An content of the center of the well-zoned plagioclase grains of Calamba are generally An_{43-50} (figure 14), although two grains contain higher An concentrations in the center: An_{65} and An_{84}. The edges of all the grains have An_{39-45}. The well-zoned plagioclase grains of Bulalo contain centers with concentrations similar to Calamba, An_{44-50}, and edges of An_{33-37}, slightly less than Calamba (figure 14). One grain had a center as high as An_{55}, with an edge at An_{51}. The centers of the well-zoned plagioclase from Bijang cover a wider range of values than the other two domes, with cores of An_{36-48}, and edges of An_{31-41} (figure 14). Of the two well-zoned plagioclase grains analyzed from Olila, one showed the common trend of

decreasing An, with a core of An_{50} and an edge of An_{39} (figure 14). The other appears to be reversely zoned, with a core of An_{40} and edge of An_{50}. However, because this plagioclase may be composed of several grains grown together, the apparent reverse zoning trend may be the result of analyses that included more than one grain. One grain from Bijang also shows this apparent reverse zoning, and also may be the result of several grains grown together.

Bulalo and Olila are the only domes in which grains were analyzed from two different sized enclaves. Plagioclase grains analyzed included the needle-like plagioclase that composes the matrix, as well as larger phenocrysts. The compositions of the grains are dependent on the size and shape of the grain, as well as the size of the enclave in which the grain was located. In the Olila samples (figure 15), the plagioclase phenocryst analyzed from the large enclave contain An_{90-98}. The needle-like grains of the large enclave contain An_{45-65}. Grains were analyzed from what appeared to be a small enclave in the host, but mixed results and the poor condition of the enclave lends doubt to that interpretation. Of the three plagioclase grains analyzed from this area of the thin section, one contained a core of An_{84} and an edge of An_{54}, one had points of An_{40-46}, similar to grains in the host, and one contained a core of An_{49} and an edge of An_{54}. This grain had a well-defined outer rim.

In the Bulalo samples (figure 15), the phenocrysts and needle-like plagioclase from the larger enclave plot in the An_{65-78} range. Four grains were analyzed from the smaller enclave in the host. The two needle-like plagioclase grains contained An_{70-75}, while the two larger phenocrysts had centers at An_{74} and An_{45}, and edges at An_{49} and An_{23}.

15

In the Calamba samples, only one large phenocryst and one needle-like plagioclase grain were analyzed (figure 15). The larger phenocryst has a center with An_{90}, and an edge at An_{72}. The needle-like plagioclase grain contains a concentration around An_{72} as well. One analyzed grain (Enclave Plag #1-24) came from an area on the thin-section interpreted to be part of a small enclave surrounded by the host, but it may instead be part of a cumulate representing the magma chamber wall. Pyroxenes analyzed from the same area of the thin section are not in equilibrium with the other pyroxenes in the host, as determined using QUILF for thermobarometry (see below). Despite this, the plagioclase grain has a concentration of An_{44-46}, which is similar to the host plagioclase grains.

The Ba concentrations in the plagioclase grains increase from center to edge, whereas Sr decreases, which results a decrease in the Sr/Ba ratios across host plagioclase from center to edge. The Sr/Ba ratios from the centers of the well-zoned plagioclase from Calamba range from 2.2 to ~4.3, with edges decreasing to 2.2-3.0 (figure 16a). The two grains with high An centers have identical Sr/Ba ratios of 6.2, and edges similar to the other grains from Calamba. The centers of the well-zoned plagioclase from Bijang have Sr/Ba ratios between 2.2 and 3.4 (figure 16a), with the edges decreasing to around 1.9. The Sr/Ba ratios for the centers of the Bulalo plagioclase are 4.0 (figure 16a), with the exception of one grain with a core at 6.0. The edges of the grains are all around 2.0. While no well-zoned grains from Olila were analyzed for trace elements, one grain that was analyzed across from rim to rim contained edge values at 2.7, and mid-points as high as 4.0.

Two grains were analyzed from the smaller enclaves of both Olila and Bulalo (figure 16b). The Sr/Ba ratios from the grains of the Olila enclave are ~4.0, similar to the values of the plagioclase grains from host plagioclase. This supports the previous conclusion that the area interpreted to be a small enclave most likely is not. The centers of the Bulalo enclave plagioclase grains are 6.0 and 6.5, similar to the values of the centers of the grains from Calamba and Bulalo with high An concentrations in the centers. A point closer to the edge of one of the enclave grains shows a large decrease in the Sr/Ba ratio, and plots with the edges of the host plagioclase grains.

Amphiboles

The amphiboles analyzed from each dome are all hornblendes based on their composition. Ternary graphs of the major element concentrations of the amphiboles (figure 17a) show very little variation between the domes. The few amphibole grains analyzed from the enclaves are similar in composition to the host amphiboles. A comparison of magnesium numbers vs. SiO_2 between the hornblende grains from the domes and the enclaves does not show a trend (figure 17b).

Pyroxenes

There is not much variation in the chemical composition of the pyroxenes among the domes (figure 18a). A comparison of the amount of enstatite present in the pyroxene grains with the Mg number of the grain also does not reveal a trend (figure 18b). All four domes contain orthopyroxene of composition $Wo_{1.3-3.9}$ $En_{68.4-70.6}$ $Fs_{27.5-29.9}$. Calamba was the only dome in which clinopyroxene (cpx) was observed and analyzed. It is possible that the other domes also contain trace amounts of cpx, but none were observed with the microprobe. The cpx present in the Calamba samples ranges from $Wo_{40.7-43.4}$ $En_{43.2-45.3}$

$Fs_{13.0-15.0}$. One grain contains a slightly different composition of $Wo_{34.8} En_{52.1} Fs_{13.1}$. Thermobarometry could only be done for Calamba because of the lack of two different types of pyroxenes in three of the domes,.

Calamba was also the only dome that contained both magnetite and ilmenite, so both of these systems were used to determine the final temperature of the Calamba magma prior to eruption. Following the procedure outlined in Andersen et al. (1993), QUILF version 4 was used to model the temperature. Of the grains analyzed, only two were ilmenite, and the compositions of these two grains were different. The magnetite grains also contained slightly different compositions, so several combinations of magnetite and ilmenite were used in order to get the best results. The results are summarized in Table 2. The calculated temperature was 854°C, with an uncertainty of ±64°C. The compositions of pyroxenes analyzed were also slightly different. The temperature calculation that gave the least amount of error using only the pyroxene system was 956°C, with an error of ±15°C. Combining the two systems resulted in a temperature of 749°C, and an error of ±48°C. With such a wide range of calculated temperatures, it seems likely that the minerals were not equilibrium with each other. Therefore, the temperature cannot be accurately calculated.

Matrix Glass

Glass was analyzed from the matrix of the host samples as well as from the enclaves of Bulalo and Olila. Generally, K_2O content increased with increasing SiO_2 content, while MgO decreased with increasing SiO_2 (figure 19). The glass analyzed from the enclaves had compositions that varied depending on the size of the enclaves. Glass analyzed from the smaller enclaves from Bulalo and Olila contain SiO_2, MgO and K_2O

concentrations similar to the host matrix glass, indicating interaction between the host and the intruding mafic magma. Glass analyzed from the large enclave from Olila plotted in the low SiO_2 range of 52-55%, indicating little or no interaction with the high-silica magma.

Oxygen Isotope Data

Data were collected from magnetite and hornblende grains from Calamba, Bijang and Bulalo in order to determine the whole rock $\delta^{18}O$ values for each dome (table 3). The $\delta^{18}O$ values collected from each mineral type were similar among the three domes (figure 20). The magnetite values varied by less than 0.12 between Bulalo and Bijang, and less than 0.5 for Calamba. The hornblende values were also very similar, with a difference of less than 0.25 among all three domes. Whole rock $\delta^{18}O$ values for the domes were calculated using an assumed temperature of 950°C, following the procedure from Clayton et al. (1989). The calculated whole rock $\delta^{18}O$ values for the three domes were also simlar. Bulalo contained $\delta^{18}O$ of 5.9 ‰, Calamba 6.29‰, and Bijang was measured at 6.06‰. The similarities of the $\delta^{18}O$ values of the mineral phases and the whole rock indicate that the minerals used in the calculations were in equilibrium with each other. This is important because it indicates that oxygen values from the minerals have not been reset, and therefore reflect the values of the source rock (Bindeman and Valley, 2003).

DISCUSSION

Comparison of the Domes and Makiling

The domes from this study occur in close proximity to volcanic deposits from Mt. Makiling. The domes are located on the south and southwest flanks of the mountain, and the major element compositions are very similar to various Makiling deposits. The majority of the volcanic products of Mt. Makiling are basaltic-andesite to andesite, although smaller amounts of trachydacite and dacite compositions are also present (Cruz, 1992). Major elements of the samples from the domes overlap the composition of samples from Makiling (figure 21a). The trace element compositions of the mafic enclaves found in the domes and the low-silica samples of Makiling are also very similar (figure 21b). The silicic samples from Makiling do not have the same concave upward trend in the REEs that the domes have, indicating that the Makiling samples are not as depleted in the MREEs as the host dome samples. Cruz (1992) presented chemical analyses of the lavas in the Mt. Makiling-Banahaw complex, and he concluded, based on major and trace element variation, that the high-silica magmas of Makiling were related to the low silica magmas through a process of fractional crystallization and assimilation. He observed that fractional crystallization alone could not account for the chemistry of the samples, including the high concentrations of Th, Ce, Zr, Hf and Sm. He proposed that the assimilation of ~5% granite/upper crust compositions could account for this composition.

Fractional Crystallization vs. Partial Melting

Several studies have examined the fractionation products of magma types commonly found in arc areas (figure 22). Grove et al. (2003) experimented with water-saturated basalts at 200 MPa, while Muntener et al. (2001) experimented with basalts containing 2 and 3% water and at 1 and 2 GPa of pressure (figure 22). Grove et al. (2003) also modeled the fractionation of a water-saturated Mg-andesite at 200 MPa. One of the difficulties in producing the silicic magmas in the domes and Makiling is that the K_2O/Na_2O values are much higher than those produced in the experiments. One trend that approaches the ratios of the domes and Makiling came from the fractionation of water saturated Mg-andesite at a near-surface pressure (Grove et al., 2003). However, the extensive fractionation required to produce high silica magmas would be unlikely to have occurred at this shallow depth. Another trend that approaches the ratios of the domes was produced through the anhydrous fractionation of a tholeiitic basalt at 1.0 GPa (Villiger et al., 2004). However, these values were only reached after extremely high amounts of fractionation had occurred, over 90%.

Beard and Lofgren (1991) and Patino-Douce (2000) have examined the products formed by the partial melting of various types of source rock. The products formed through the melting of a meta-basalt (Patino-Douce, 2000) do not contain K_2O/Na_2O ratios that are similar to the high-silica magmas from the domes and Makiling (figure 23). Partial melting experiments beginning with meta-andesite to dacite compositions, however, did produce products with ratios similar to the domes (Patino-Douce, 2000). In this case, the K_2O/Na_2O values produced are high enough, but the $Na_2O + K_2O$ is low. Experiments in which the starting composition is a calk-alkaline andesite, such as those

found in the Corridor (Cruz, 1992) may be able to produce both the high K_2O/Na_2O ratios and the $K_2O + Na_2O$ values of the domes. There have been no published experiments involving the partial melting of calc-alkaline andesites similar to the ones found in the Macolod Corridor.

Eu-anomalies are often used as an indicator of evolution by fractional crystallization. In order for significant amounts of high-silica magma to be produced, large amounts of plagioclase would have to be fractionated out (Price et al., 1999). This would cause a noticeable negative Eu-anomaly. No negative Eu anomaly is observed in the domes (figure 13). However, if the magmas were produced in an oxidizing environment, Eu would occur as Eu^{3+}, and would not be partitioned into plagioclase. Therefore, no negative Eu anomaly would be observed. Because most arcs are oxidizing environments, this may explain the lack of a Eu anomaly. Plagioclase fractionation also leads to a large depletion in the concentration of Sr in the more evolved samples because Sr is strongly partitioned into plagioclase. Estimates of the partition coefficient for Sr into plagioclase range from 2.8-15.6 (Rollinson, 1993). The removal of the large amounts of plagioclase required to reach high silica values should greatly deplete the amount of Sr in these samples. The concentration of Sr in the host samples fall between 200 and 400 ppm, which seems to be too high to indicate evolution by fractional crystallization (figure 13).

The composition of individual plagioclase grains has frequently been used to trace processes occurring in magma chambers. The slow diffusion rate of Na and Ca through the grains makes them an ideal indicator of how the chemistry of a magma changes (Singer et al., 1995; Tepley III, et al., 1999; Ginibre et al., 2002; Browne et al., 2004).

The changing chemistry of a magma chamber should be recorded in the plagioclase grains, with a high-anorthite core (An_{75-95}) indicating the grain began growing in a more mafic magma, and decreasing anorthite towards the rim indicating a magma that is becoming more silicic (Gertisser et al., 2000). However, other processes occurring in the magma chamber can affect the major element composition of the plagioclase grains, including changes in water pressure and temperature, as well as magma mixing (Ginibre et al., 2002; Browne et al., 2004). The trace element concentration in a grain, particularly Ba and Sr, can help differentiate between these processes. The partitioning behavior of Ba and Sr between liquids and plagioclase grains have been well-defined (Blundy and Wood, 1991), and are not affected by the same processes as the major elements. Because the Sr/Ba ratio reflects the change in anorthite across the grain (figure 24), the changes in the chemistry of the grain are due to compositional changes in the magma chamber rather than water pressure or temperature changes (Blundy and Wood, 1991; Browne et al., 2004).

Fractional crystallization occasionally produces plagioclase grains with large variations in An concentrations across the grain (>20%), and cores that indicate a mafic origin for the grain (Singer et al., 1992; Watts et al., 1999; Gertisser et al., 2000). In these studies, although these grains were present in the assemblages, they were rare. In the dome samples, Calamba is the only one which contains plagioclase grains (2) that have changes in An content of more than 20% from center to edge. In the other three domes, no large changes in composition were observed. The Sr/Ba ratio in the cores of the grains would also record an origin in a less evolved magma. Only 3 grains in the host

domes contain centers with much higher Sr/Ba ratios than the other host grains- the 2

grains from Calamba and one from Bulalo (figure 16a).

Magma mixing

Mingling and mixing between the more mafic magma represented by the enclaves

and the host silicic magmas of the domes did not play a major role in the generation of

the dome magmas. The chemical compositions of the minerals do not indicate much

interaction between the silicic host and more mafic magma. There is no evidence that

grains were shared between the two magma types, as would be expected if they had been

in contact for a significant amount of time (Snyder and Tait, 1998). Also, reversely-

zoned plagioclase grains are not found in the host, and normally zoned plagioclase that

show a great decrease in An content from the center to the edge are very rare. The rims of

the plagioclase are in equilibrium, as indicated by the similar composition, and do not

contain the increase in anorthite content or Sr/Ba that would be observed due to

prolonged contact with a mafic magma.

There is also little textural evidence for magma mixing. Sieve textures and

reaction rims on minerals are very rare in the samples, except along boundaries between

the host and enclave, as well as in the smaller enclaves. Also, analyses taken from these

sieve-textured cores, including the An-content and Sr/Ba ratios, were not different from

the cores of the other grains (e.g. Calamba Plag #1-24). This compositional similarity

indicates that the sieve-textured cores present may be the result of other processes in the

magma chamber that caused disequilibrium between the grain and the liquid, and lead to

partial dissolution of the grain. These processes could include a change in temperature or

pressure within the chamber. The rims that are present on the plagioclase grains are thin,

24

even along the boundaries between the enclaves and host. The widest rims are found in the smaller enclaves, indicating more interaction with the host. There is no evidence of mingled glass in the host. The glass analyses from the matrix of the host contain a SiO_2 content that is higher than the bulk SiO_2 content (figure 19). Glass analyzed from the larger enclave of Olila has a SiO_2 content that was similar to the bulk silica content of the enclave, indicating little, if any interaction with the host magma. Glass analyzed from the smaller enclaves contained much higher SiO_2 values, indicating more interaction with the silicic magma.

Eruption of the magma/formation of the domes

I propose a model for the formation of the dome and the high-silica Makiling magmas involving the partial melting of discrete batches of previously emplaced calc-alkaline andesitic magma (figure 25). In this model, the first step involves melting of the mantle wedge as the result of the subduction of the Eurasian plate. The magmas produced in this manner travel through the wedge and pond at the base of the lower crust, where they may remain partially molten. From experimental petrology, we know that basaltic magmas could not produce the composition of the dome magmas, it is likely that these ponded, crystallized magma batches are calc-alkaline andesite (or dacite) in composition. In the next step, influxes of basaltic magma produced in the mantle wedge encounter the solidified magma body, partially melt it, and mobilize the more silicic melt. This siliceous melt travels through the crust and forms a magma chamber, possibly in the upper crust. There is little interaction between the silicic magma in the chamber and the wall-rock surrounding it, because interaction with rocks in the upper crust would raise the oxygen isotope ratios to values above the mantle values observed in the dome samples

(Bindeman and Valley, 2003). In the third step, hot, mafic magma is injected into the silicic magma chamber, causing a rapid eruption due to an increase in pressure and temperature in the magma chamber. The extensive faulting in the Macolod Corridor most likely creates weaknesses in the crust, making it easier for the magmas to reach the surface. These magmas then erupt, forming the domes. The contact between the mafic and silicic magma in the chamber is relatively brief, as the lack of any evidence of mingling or mixing between the two magma types suggests.

The processes that formed the four domes examined in this study were probably very similar, which led to the similar chemical compositions and mineral textures among the four domes. The differences between Calamba and the other three domes could be the result of source magmas with different chemical compositions, or different processes. However, the similar $\delta^{18}O$ values among Bulalo, Olila and Calamba suggest that each originated from a similar source. One difference between them may be the depth that each magma formed at, because amphibole has a very strict depth limit at which it can form. Because Bulalo, Olila and Bijang all contain significant amounts of amphibole, it is also possible that the source magmas for those three domes were more hydrous than the magma of Calamba. One other possibility is that the Calamba magma formed due to higher degrees of partial melting. The lower concentrations of silica, and higher concentrations of Al_2O_3, MgO, FeO, CaO and Na_2O support this. The higher Dy/Lu ratios of the Calamba samples provide further evidence of a higher degree of partial melting, providing that the source contains large amounts of amphibole. Higher degrees of partial melting of an amphibolitic source would lead to a greater concentration of MREEs in the resulting magma. More partial melting of a source would also lead to a

26

lower concentration of LREEs. An initial melt would be highly concentrated in the incompatible LREEs, which would become more dilute after further partial melting events.

The domes and the high-silica magma from Makiling are most likely not related. The lack of similarities between the trace elements of the domes and Makiling indicates that while it's possible that the processes that formed them were similar, it is likely that the source magmas were different. Further data collection could determine more exactly how these areas are related, particularly oxygen isotope data from the Makiling silicic magmas.

CONCLUSION

The majority of the evidence presented in this study indicates that partial melting of previously emplaced discrete andesitic bodies located in the lower crust formed the high-silica magmas of the domes. Fractional crystallization of a magma body can not account for the compositions of the dome magmas. The K_2O/Na_2O ratios can not be reproduced by fractional crystallization alone. The Sr values of the whole rock are too high to account for the large amounts of fractionation required to form significant amounts of high-silica magma. Textural and chemical data do not indicate that magma mixing and mingling played a major role in the creation of the dome magmas. They show, instead, that the mafic magmas represented by the enclaves were not in contact with the silicic magma for a significant length of time.

APPENDIX 1

PETROGRAPHIC DESCRIPTIONS

Petrographic Analyses

Bijang

The samples from Bijang are porphyritic, with 15-25% phenocrysts and a glassy, microlitic matrix. Plagioclase is the most abundant mineral in Bijang, constituting around 60% of the phenocrysts. The phenocrysts range in size from 0.2 to 2.7 mm, with an average of approximately 1 mm and a normal grain-size distribution. Any plagioclase grain with a length less than 0.1 mm was considered part of the matrix (in all four domes). The grains are mostly twinned and euhedral with most showing rounded edges and slight embayments, which may indicate partial resorption. Grains with a sieve texture throughout are rare. Most of the larger grains are well-zoned, and some of the smaller grains also show zoning. Rarely, grains show a sieve texture core and a well-zoned rim. Glomerophyric clots consisting of two or more grains of plagioclase that have grown together are present in the samples. In these clusters, the outer edges of the plagioclase contain slight resorption features. These clusters occasionally contain other minerals, including amphibole and opaques. These may be pieces of the wall rock that were taken up during the eruption and not part of the host magma.

Hornblende is the next most abundant phenocryst, constituting about 30% of the phenocrysts. The grains are mostly euhedral with some subhedral grains. They range in size from 0.13 to 0.7 mm, although the larger grains are rare. Most are in the 0.2-0.4 mm range. Smaller grains are present in the matrix (< 0.1mm), but in much smaller quantities than the plagioclase. The hornblende grains often display some resorption features, with rounded edges and slight embayments. Hornblende grains with disequilibrium textures

such as an extremely sieved texture and large embayments are rare. Reaction rims were not observed on the hornblende grains.

Opaque grains are found throughout the samples, in the matrix as well as in phenocrysts as inclusions, and constitute ~5% of the phenocrysts. The shapes vary from euhedral to anhedral, and the grains do not contain embayments. The larger grains are approximately .66 mm, although most are much smaller. Orthopyroxene is the least abundant mineral in Bijang, composing 3-4% of the phenocrysts. The grains range in size from 0.28 mm to less than 0.06 mm. The larger grains are rare, and most of the grains are around 0.1 mm or smaller. The pyroxenes are mostly euhedral and few show signs of resorption. Biotite is also present in the samples in very trace amounts, as inclusions in the hornblende.

Bulalo

The mineralogy of Bulalo is very similar to Bijang, although Bulalo contains mafic enclaves. The samples from Bulalo are porphyritic, with a phenocryst content of 20-25% and a glassy, microlitic matrix. The matrix contains brownish areas that most likely are areas of devitrification. Plagioclase is the most abundant phase, constituting ~65% of the phenocrysts. The phenocrysts range in size from 0.17 to 2.16 mm, with an average of ~1 mm and a normal grain-size distribution. The grains are commonly twinned, and are euhedral to subhedral. Many show slight resorption features, such as rounded edges and slight embayments. Grains with a sieve texture are present, but rare. Grains with sieve-textured cores and well-zoned rims are also rare. Zoning is common in the grains, especially in the smaller ones. Some grains display well-developed outer rims

31

that may represent contact with a magma of a different composition, but these are not common in the host plagioclase. Glomerophyric clots consisting only of plagioclase are present but rare, as are clots containing other mineral types. These minerals include hornblende, magnetite, and orthopyroxene (as rare inclusions in the hornblende).

Hornblende is the second most abundant phase, constituting about 25% of the samples. The grains are euhedral to subhedral. The hornblendes range in size from about 0.18 to 0.70 mm with an average of 0.25 mm. Larger grains of hornblende are rare. Smaller grains are found in the matrix. Many of the non-matrix hornblende grains show signs of resorption, including rounded edges and slight embayments. The hornblendes rarely contain a sieve texture in the core, or throughout the grain. Reaction rims were not observed on the hornblende grains.

Orthopyroxene constitutes ~5% of the phenocrysts. The grains range in size from 0.05 mm to 0.27 mm, although most of the grains are small, between 0.08 and 0.1 mm. The grains are mostly euhedral and show little evidence of resorption. The resorption features are more common in the large grains than the small ones. Opaque grains compose 3-4% of the samples. The shapes of the opaques range from euhedral to anhedral. The grains are not embayed. The largest grains are around 0.32 mm, with an average of 0.05 mm.

The mafic enclaves found in Bulalo are various sizes, but the mineralogy is the same. Some of the enclaves are fist-sized and could be sampled individually, composing the mafic samples from Bulalo. Some of the enclaves are very small, and are included in the host samples. The enclave features a noticeable change in texture from the host, with the matrix being composed of needle-like plagioclase, with sizes from 0.46 mm to

<0.1mm. The average size is ~0.3 mm. The smaller enclaves contain matrix plagioclase that are generally smaller, 0.39 mm long and 0.09 mm wide. The grain size is the only difference among the different sized enclaves. The mineralogy is the same, with 50% plagioclase, 45% hornblende and 5% opaques. Some of the plagioclase grains show distinct rims. Larger, plagioclase phenocrysts are present in the enclave, but rare. These are up to 0.39 mm long. The hornblende in the enclaves is almost as abundant as the plagioclase, with a size range that is from 0.03 mm to 1.25 mm. Many of the grains are anhedral and fill in the space between the plagioclase grains, while others have an elongate, euhedral shape. Some of the hornblende grains have a sieve texture, although this is not common. Opaque grains are scattered throughout the enclave, and constitute ~5% of the phenocrysts. The size and shape of the opaques vary, with no dominant shape. The average size is around 0.05 mm. There are no resorption features on these grains. Glass is present in small amounts in the enclaves.

Olila

The samples from Olila are porphyritic, with phenocrysts constituting 20-25% of the samples, and a glassy, microlitic matrix. Mafic enclaves are also present in the Olila samples. There are some brown areas that may be the result of devitrification. Plagioclase is the most abundant phase, constituting ~68% of the phenocrysts. The grains range from 0.15 to 2.16 mm, with an average of ~1 mm and a normal grain-size distribution. Most of the grains are twinned and euhedral, and most show signs of resorption. Some plagioclase grains are subhedral due to what appears to be deep embayments. A few grains in the host also display cores with sieve textures and well-

zoned rims. Some appear to have well-developed outer rims on them. Most occur as single grains, with rare glomerophyric clots consisting of only plagioclase. Clots containing plagioclase, hornblende, opaques and orthopyroxene are rare as well. They may represent wall rock from the chamber.

Hornblende constitutes ~ 25% of the phenocrysts in Olila. The grains are generally euhedral, although most of them have rounded edges and slight embayments. The hornblendes have a large range, from ~ 0.09 to 2.0 mm. They average 0.9 to 1.1 mm. Small (< 0.1 mm) grains were observed in the matrix. The non-matrix hornblende grains rarely contain a sieve texture throughout. Most of the large grains contain inclusions of plagioclase and opaques. No reaction rims were observed on the hornblende grains of Olila.

The opaque grains make up 5% of the phenocrysts of Olila. They are found in a variety of shapes, ranging from euhedral to anhedral. The grains do not typically contain embayments, although some were observed on the larger grains. The larger grains are approximately 0.32 mm in diameter, although most are much smaller. Orthopyroxene is the least abundant phenocryst in Olila, constituting ~3% of the phenocrysts. The grains range in size from 0.04 mm to ~0.58 mm, although the larger pyroxenes are rare. Most of the grains are 1 mm or less. The shapes of the grains are euhedral to subhedral, and slight embayments occur rarely.

The Olila samples contain enclaves of varying sizes with a mineralogy similar to the enclaves of Bulalo. The mineralogy of the different sized enclaves is the same, but the grain sizes are slightly different. Generally, the matrix of the enclaves is composed of needle-like plagioclase grains. The lengths of the matrix plagioclase of the larger

t

g

an

ph

$25°$

sam

Cala

the s

Grai

with

resorp

core w

texture

enclaves range from 0.07 to 0.62 mm, with widths from 0.02 to 0.05 mm. In the smaller

enclaves, the lengths of the needle-like plagioclase range from 0.04 to 0.2 mm and widths

range from 0.006 to 0.008 mm. Some of the needle-like plagioclase of the smaller

enclaves contain a noticeable rim. These are rare in the larger enclaves. The plagioclase

phenocrysts present in the smaller enclaves are not common. They are generally ~ 0.72

mm and show some zoning. Altogether, plagioclase constitutes ~50% of the minerals.

Hornblende is also found in the enclave, composing ~50% of the phenocrysts. Most of

the hornblende is anhedral and fills the space between the plagioclase grains. Opaque

grains in the enclaves range in size from 0.02 to 0.08 mm. These grains are generally

anhedral-subhedral, with some euhedral grains, and constitute only ~1% of the

phenocrysts.

Calamba

The samples from Calamba are porphyritic, with phenocrysts constituting ~20-

25% of the samples. The matrix is devitrified in most of the samples, although one

sample (020517-2d) does contain a glassy matrix. Mafic enclaves are present in the

Calamba samples. Generally, the phenocrysts in Calamba compose around 20-25% of

the sample. Plagioclase is the most abundant phase, composing 70% of the phenocrysts.

Grain-sizes of the plagioclase are normally distributed, and range from 0.08 to 2.37 mm,

with an average size of 1.2 mm. Many of the grains are twinned, and most show signs of

resorption, including rounded edges and slight embayments. Grains with a sieve-texture

core with a well-zoned rim were rare. Grains that were completely composed of a sieve

texture are also rare. In the Calamba samples, glomerophyric clots consisting only of

plagioclase grains are rare. However, clots consisting of plagioclase, clinopyroxene, opaques and orthopyroxene are common. These clots may represent pieces of the wall rock that were taken into the host magma. The size and shape of the grains in these clots is variable. Some of them contain large plagioclase grains, with all the remaining grains being much smaller. Others have large clinopyroxene and small plagioclase grains. The cumulates appear to have disaggregated.

The next most abundant phase is pyroxene, which constitutes 25% of the phenocrysts. Both clinopyroxene and orthopyroxene are present, but it is difficult to distinguish the two under the microscope. Grain size ranges from 0.05 mm to ~ 0.23 mm. Most of the grains are small, with the average of approximately 0.12 mm. Generally, the individual grains are euhedral and show no sign of resorption. However, the larger grains are often subhedral. This is possibly due to resorption, or they may be part of the disaggregated cumulate.

The next most abundant phase in Calamba is the opaque grains, constituting 3-4% of the phenocrysts. The grains are mostly anhedral to subhedral, with a few euhedral grains observed. Grain size ranges from 0.03 to 0.43 mm. Both magnetite and ilmenite are present in the samples, but they are impossible to distinguish under the microscope. The grains did not show resorption features. Hornblende is a rare phase in the host, with only a few grains identified. Those present are small (< 0.05 mm) and subhedral-anhedral.

The mafic enclaves in the Calamba samples contain a mineralogy that is different than the other three domes. The minerals present include plagioclase, hornblende, pyroxene and opaques. The matrix is composed of needle-like plagioclase. Along the

edge of the enclave that is in contact with the host, the plagioclase grains are much smaller, with sizes around 0.04 mm long and only 0.008 mm wide. Farther away from the contact zone, the plagioclase are larger, approximately 0.12 mm wide and 0.83 mm long (on average). Resorption features and well-defined outer rims are common on the plagioclase in the enclave. The larger phenocrysts of plagioclase in the enclaves are often severely resorbed, with sieve textures and deep embayments. Some of the grains have a core with a sieve texture, and a rim that is severely embayed.

The pyroxenes and hornblende in the enclaves are anhedral, and appear to have grown between the plagioclase. This makes it difficult to distinguish them visually because the cleavage planes and shapes are often missing or distorted. They are found in a much smaller abundance than the plagioclase, and often display a sieve texture. Euhedral grains of pyroxene and hornblende are present, but rare. Many opaques are present in the enclaves, but they are often very small. They have variable shapes, and some have a reddish tint around them.

APPENDIX 2

FIGURES
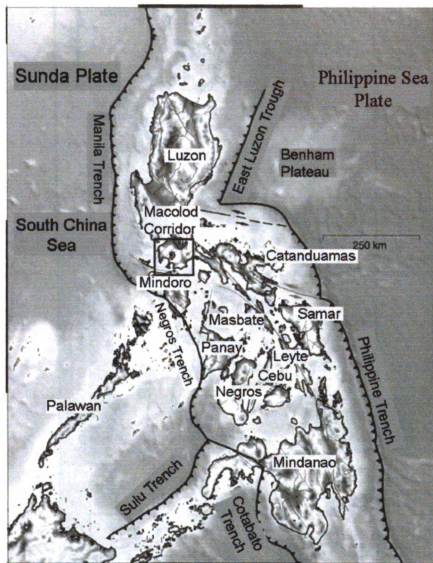
Figure 1– Map of the Philippines showing the location of the plates and the features associated with them. Note: the author refers to the Eurasian Plate as the Sunda Plate in this diagram (Bacolcol, 2003).
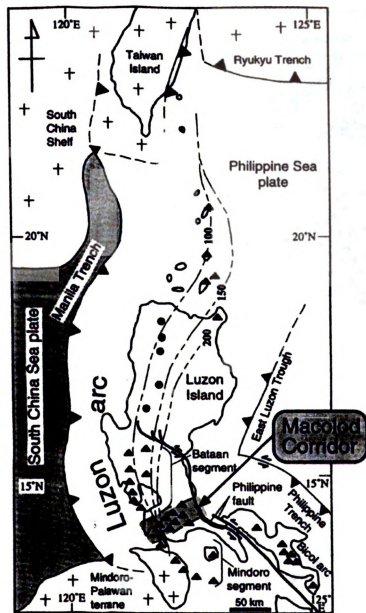
Figure 2- Location of the Macolod Corridor: It is located between the Bataan and Mindoro segments of the Luzon Arc. On this diagram, the Eurasian Plate has been labeled as the South China Sea Plate. The Mindoro-Palawan terrane in the southwest part of the islands contains a large block composed of continental crust. However, it is located well south and west of the Macolod Corridor, in which the presence of continental crust has not been observed (Defant et al., 1989).
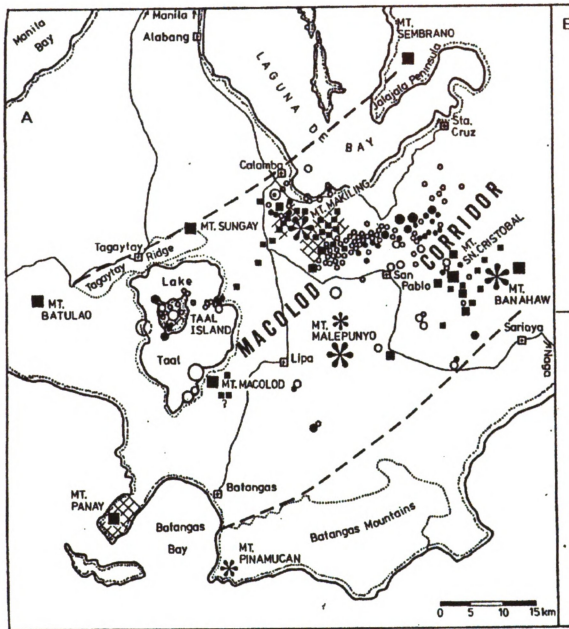
Figure 3- Location of the Macolod Corridor in relation to Taal
Volcano and the Laguna de Bay caldera (Sudo et al., 2001).

Legend:
- △ - Calamba
- ✚ - Bulalo
- ◆ - Bijang
- ✦ - Olila
- ✖ - Mt. Makiling

LAGUNA DE BAY
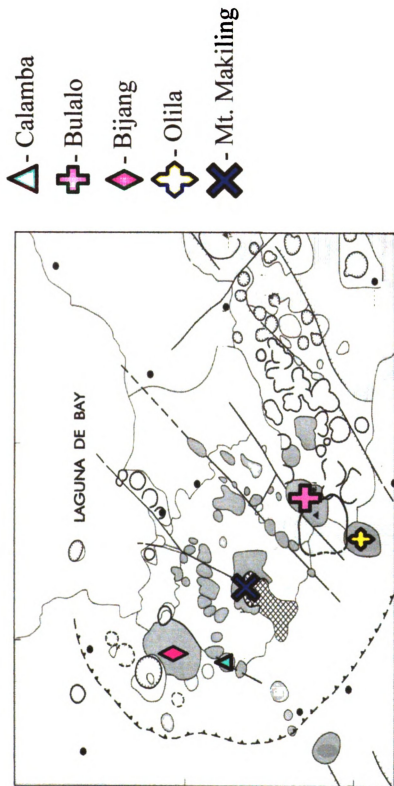
Figure 4 - Close-up view of the Makiling volcano area and the domes associated with it (Oles, 1991).

42
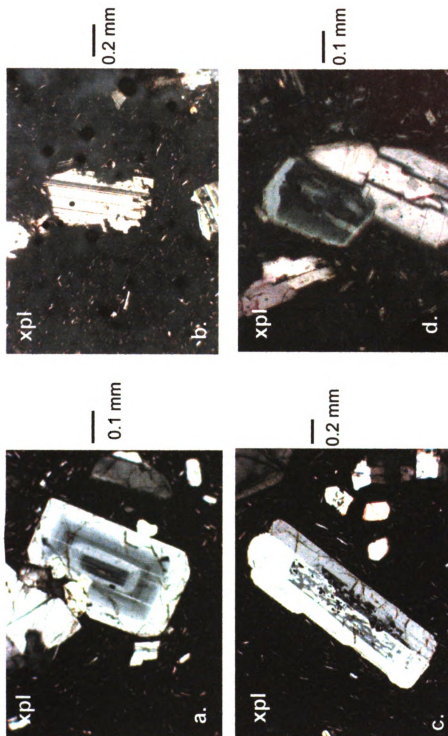
Figure 5- Examples of plagioclase grains from the four domes: a. Well-zoned grain from Calamba (020517-2d); b. Grain from Olila (020522-56tav) that is highly embayed, possibly indicative of disequilibrium; c. Grain from Calamba (020517-2d) that has a sieve-like texture in the center surrounded by a rim; d. Grain from Olila (020522-2d) with a well-defined outer rim.
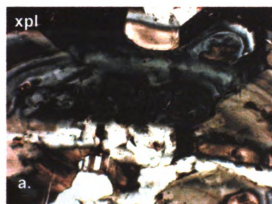
Figure 6- Example of two glomerophyric clots: a. Clot containing only plagioclase grains, from Olila (020522-53); b. Clot from Calamba (020517-2d) that contains several different mineral types grown together.
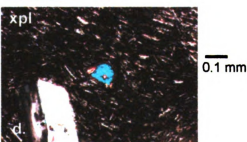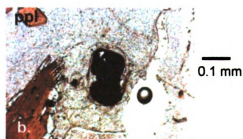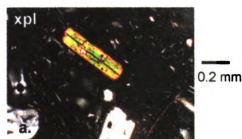
Figure 7- Examples of minerals found in the four domes- a.Common hornblende grain from Bijang (020518-1c); b. Large opaque grains from Olila (020522-53); c. Orthopyroxene grain from Bulalo (020522-51); d. Clinopyroxene grain from Calamba (020517-2m).

0.2 mm

0.2 mm
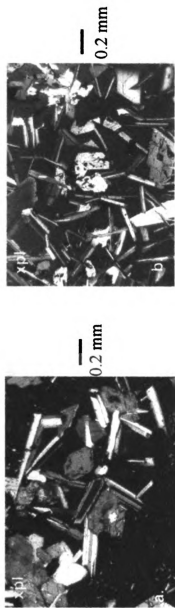
Figure 8- Examples of phenocryst differences from the two different sizes of enclaves: a. Small enclave from Bulalo (020522-51); b. Large enclave from Olila (020522-51tav)- Note the difference in the grain sizes, with the smaller enclave composed of larger needle-like plagioclase grains, most with well-defined compositional rims, while the larger enclave has smaller needle-like plagioclase grains with larger phenocrysts of hornblende and plagioclase.
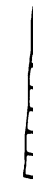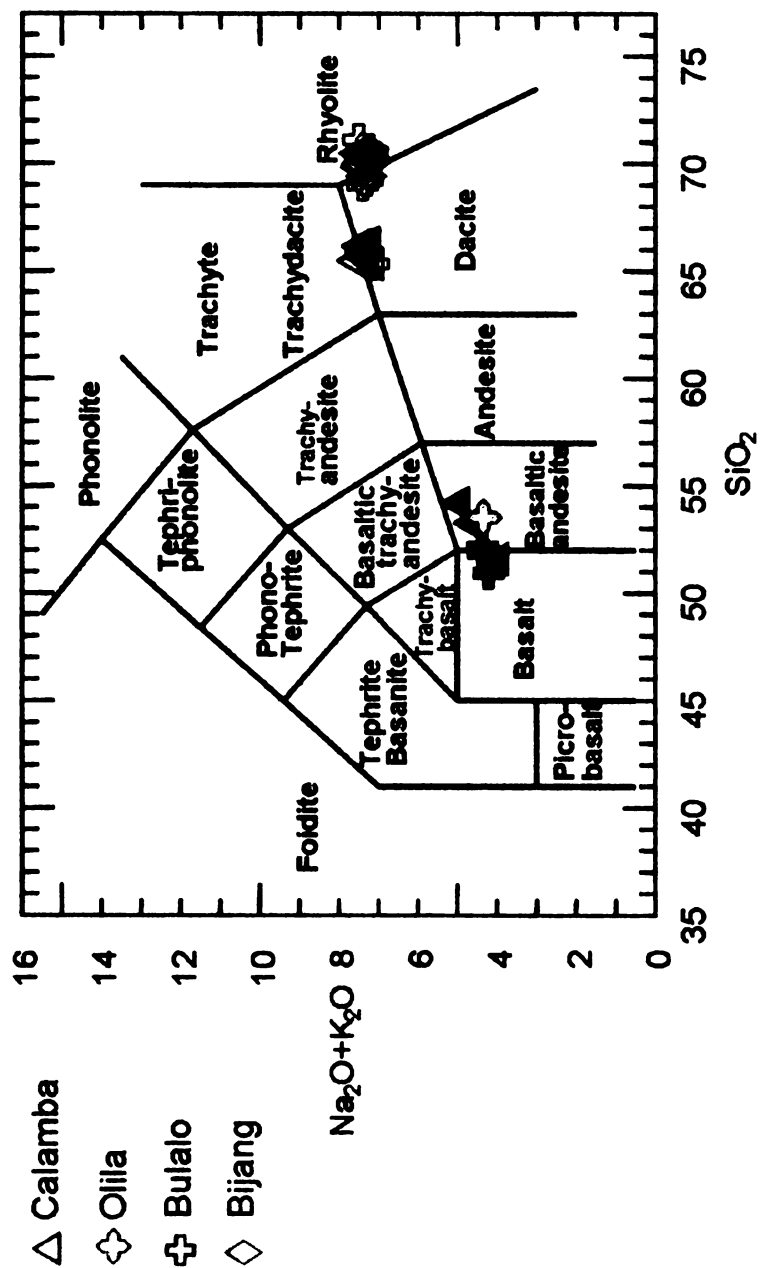
Figure 9- Bulk chemical compositions of the domes and enclaves- classifications based on Le Bas et al. (1986). Filled symbols: Enclaves; Open symbols: Domes

46

Figure 10- Major element diagrams of the host and enclave compositions. The host composition of Calamba is different than the other three domes. The enclave compositions of each dome are very similar.

△ Calamba
◇ Olila
✚ Bulalo
◇ Bijang

47
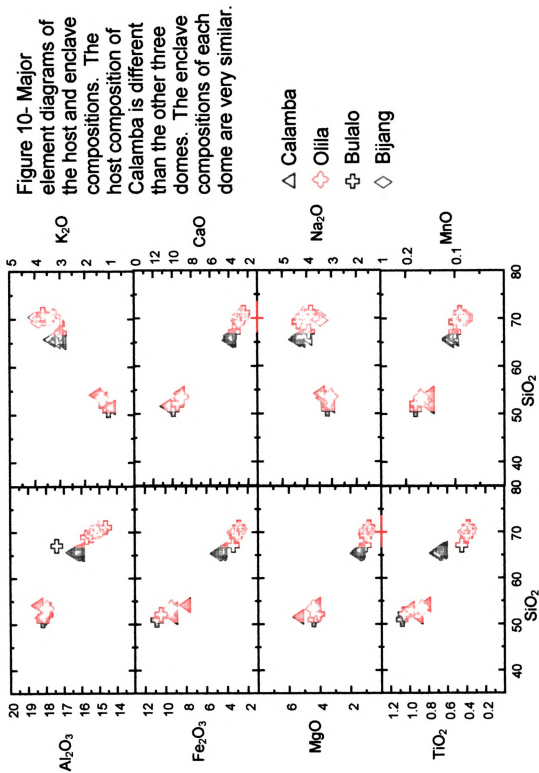
Figure 11- Trace element diagrams of the host and enclave compositions. The host compositions of Calamba display some differences compared to the other three domes.

△ Calamba
◇ Olila
✚ Bulalo
◇ Bijang
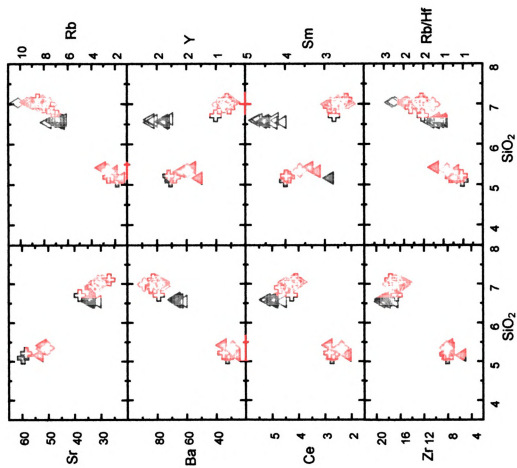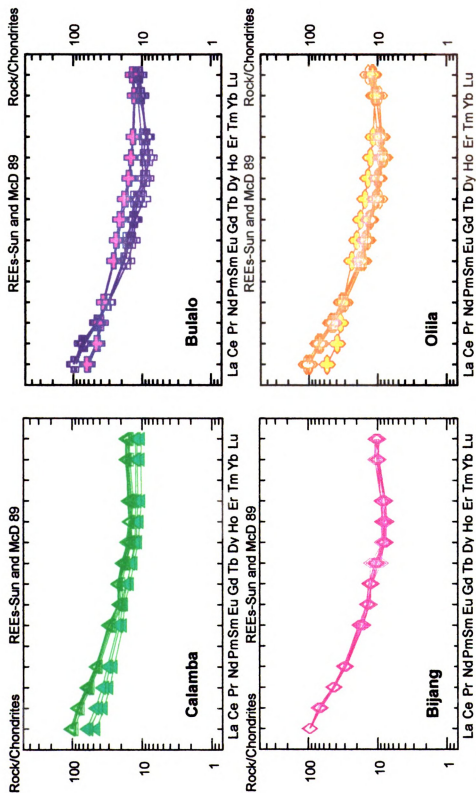
Figure 12a- REE diagrams of dome and enclave compositions, based on Sun and McDonough (1989), normalized to chondrite compositions. The host compositions of all four domes display a concave upward trend indicative of a depletion in the MREEs. The enclaves do not show this depletion, except those from Calamba.
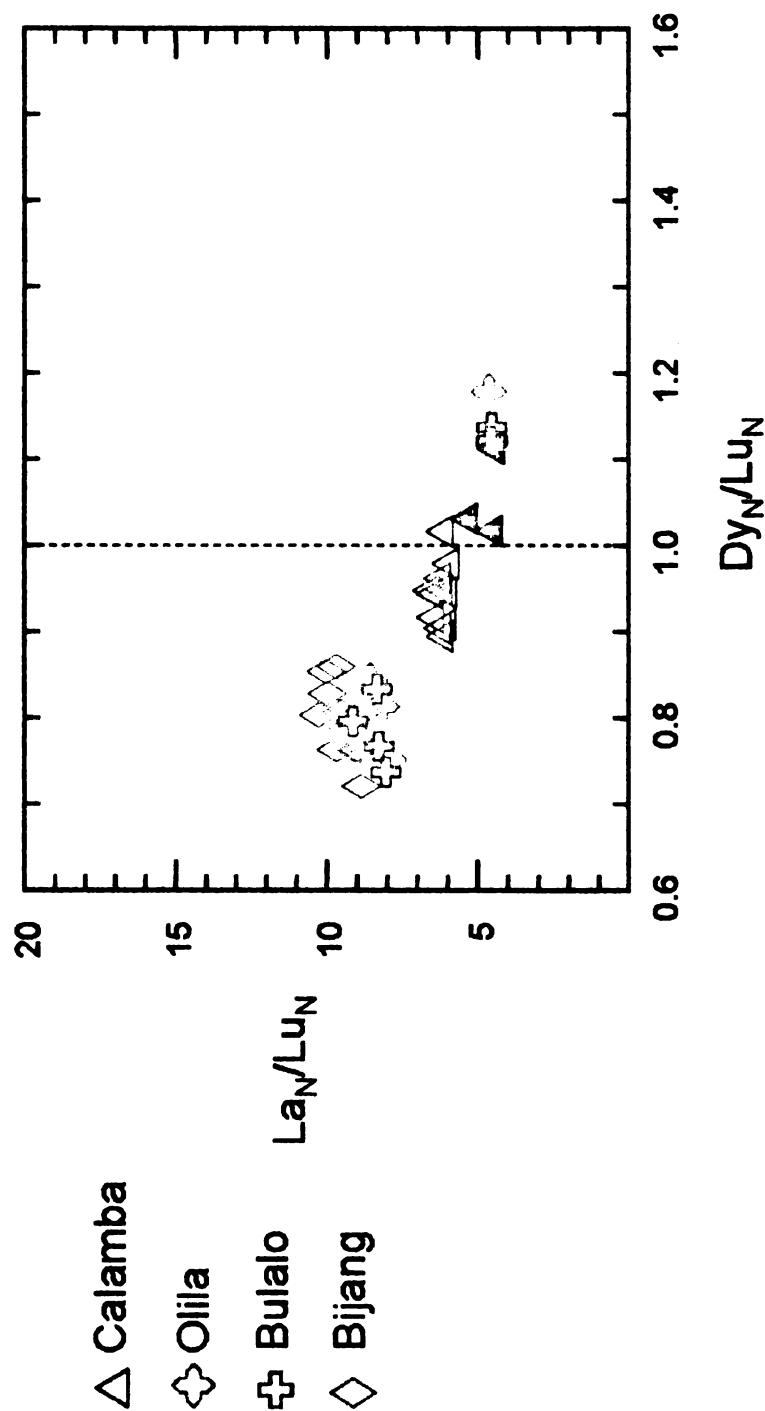
Figure 12b- Diagram showing the difference in the MREEs and LREEs between Calamba and the other three domes. The difference in MREEs may be attributed to the presence of amphibole in the source. The MREEs have higher partition coefficients into amphibole than the other REEs, and are represented by Dy on the diagram. The difference in LREEs may be attributed to different degrees of partial melting. Values were normalized to their mantle source values, per the IgPet program.
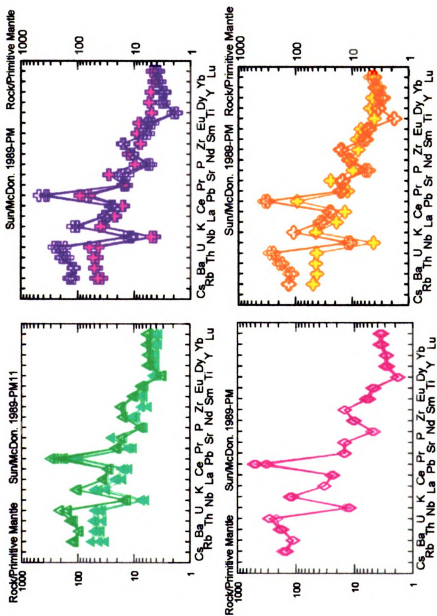
Figure 13- Trace element diagram normalized to primitive mantle, based on Sun and McDonough (1989). These diagrams show that the four domes lack a Eu anomaly.
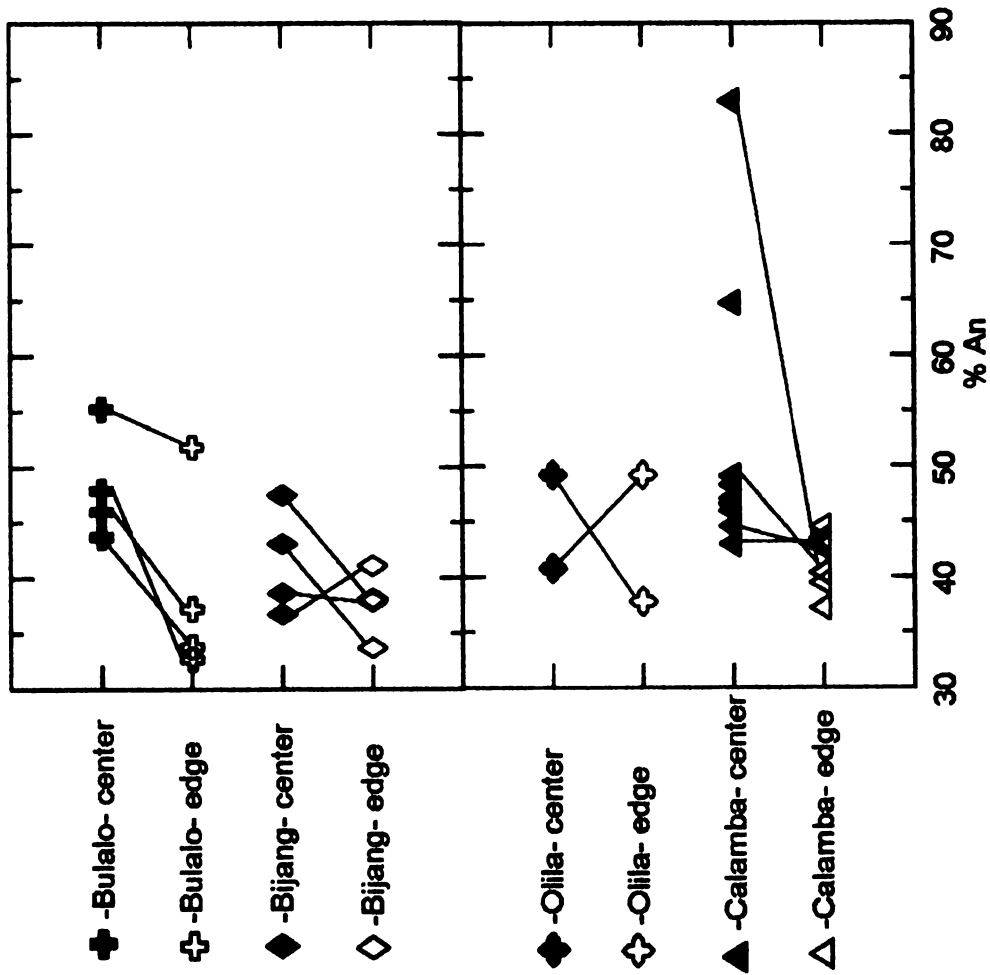
Figure 14- Diagram showing An content of plagioclase grains from the four domes. Generally, the trend is a decrease in An content from the center of the grain to the edge. One grain from Bijang and one grain from Olila shows what appears to be reverse zoning, but could also be the result of analyzing two different grains that have grown together. Also of note are the two grains from Calamba with cores of An > 55%. The tie lines connect the center of grains with the edge of the same grain.

52
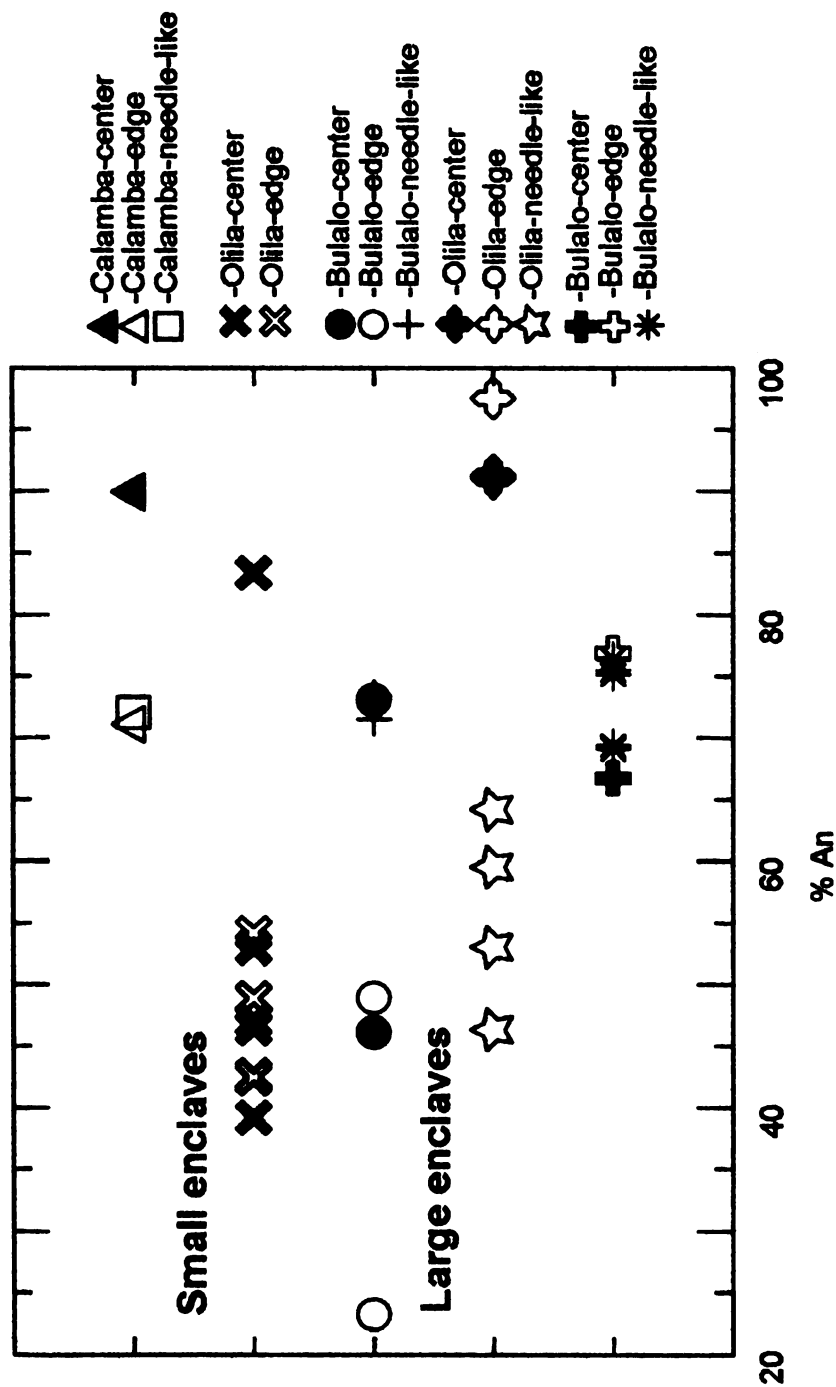
Figure 15- Diagram of An compositions of plagioclase grains from the enclaves of Bulalo, Olila, and Calamba. Bulalo and Olila contained two different sized enclaves, although it is likely that the area interpreted as a small enclave in Olila was not one, based on the low An content of the grains.
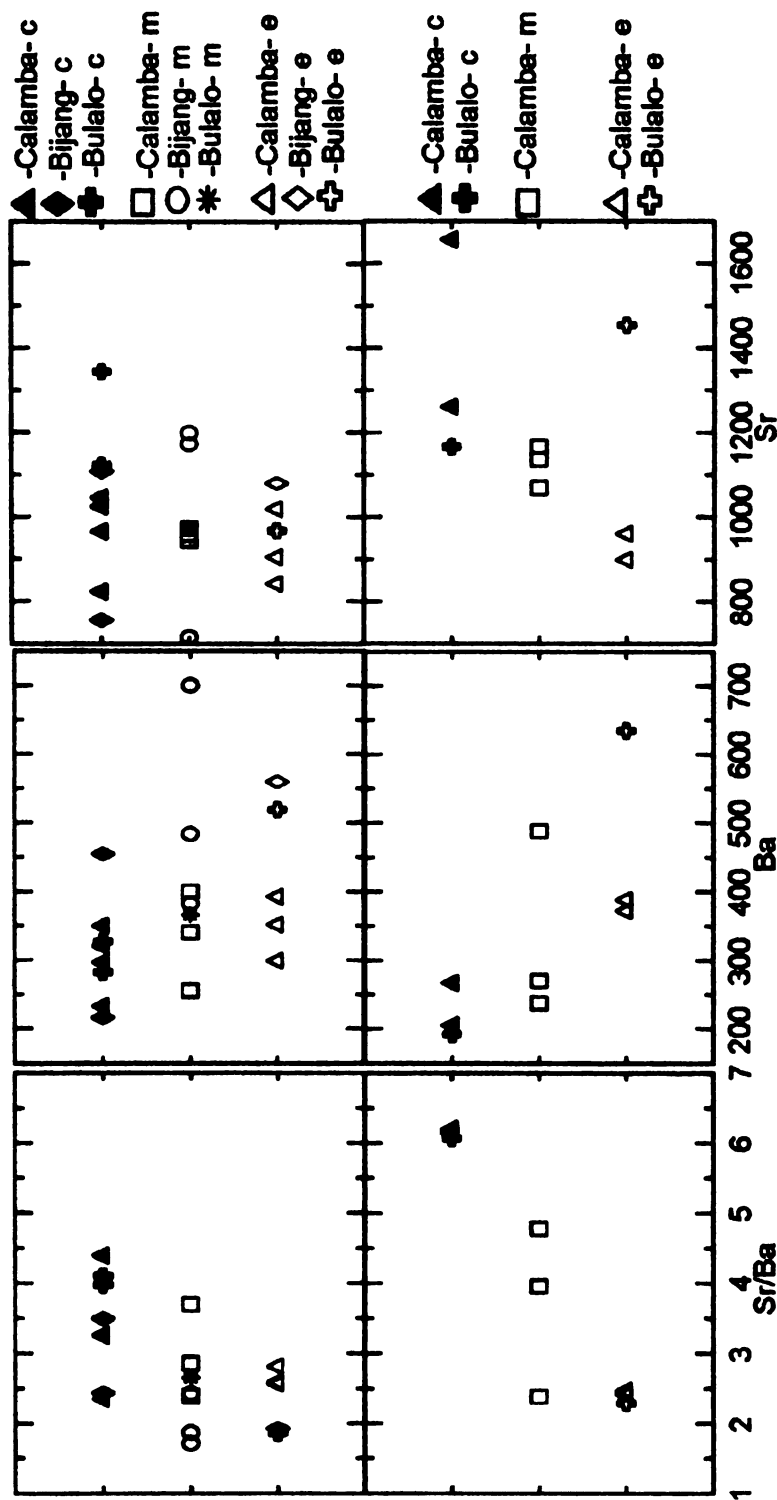
Figure 16a- Diagrams showing the Sr and Ba concentrations and Sr/Ba ratios in plagioclase grains from Calamba, Olila and Bulalo. The bottom diagrams contain data from three grains (two from Calamba, one from Bulalo) that contained centers with much higher An content than the edges. Despite the similar Sr/Ba ratio of the centers of the three grains in the bottom diagrams, the An content of the center of each one is very different: 83%, 64% and 55%.
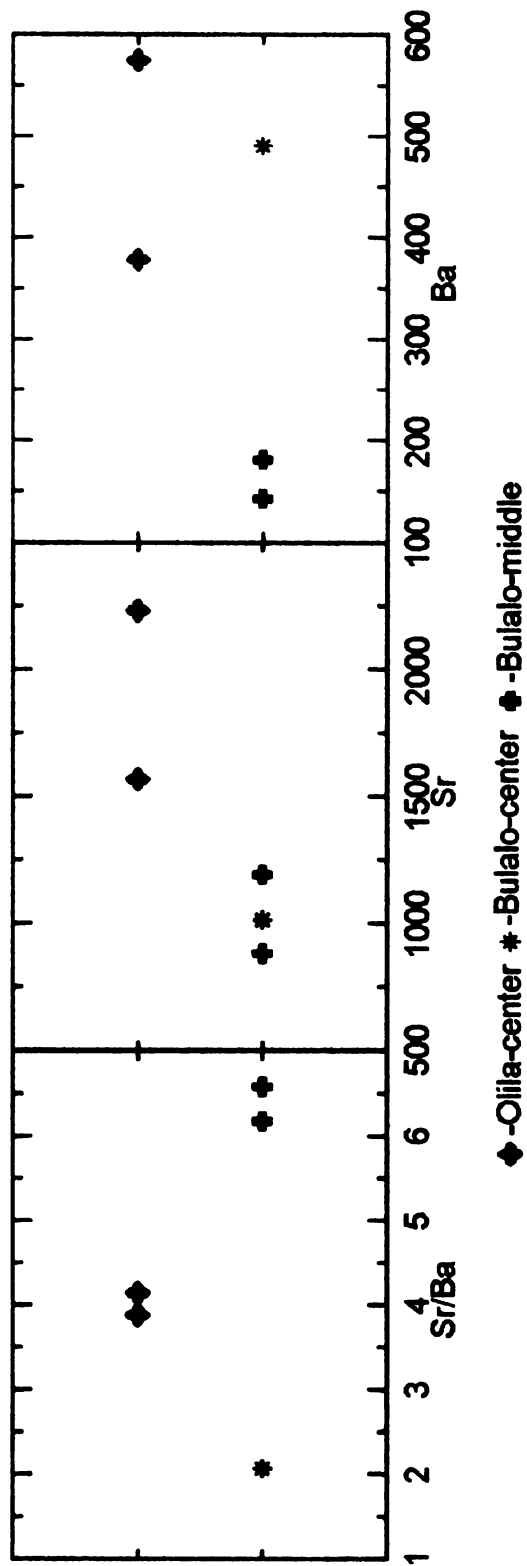
Figure 16b- Diagram of Sr and Ba compositions as well as Sr/Ba ratios of enclave grains from Olila and Bulalo. All three grains were located in small enclaves.
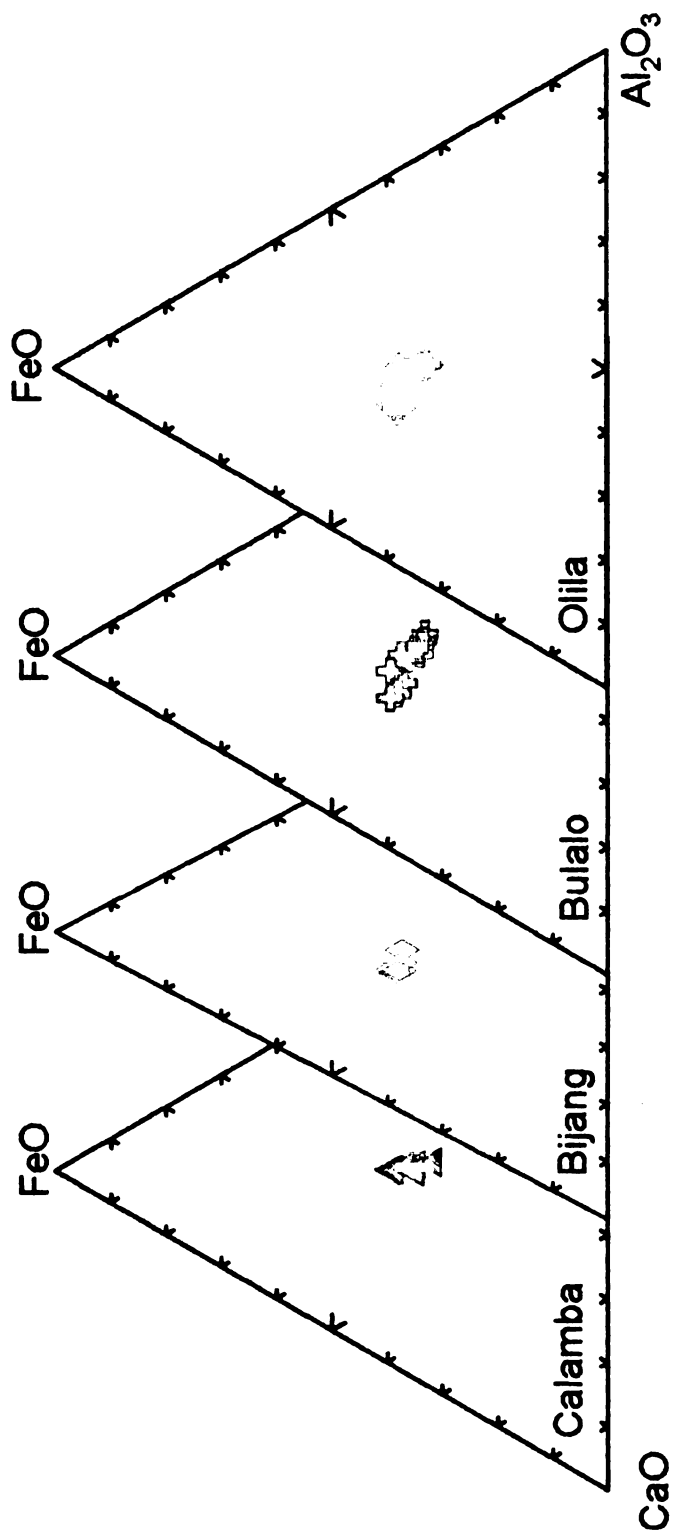
Figure 17a- Amphibole major element chemistry- there is no noticeable difference between the chemical composition of the amphiboles of the domes, or between the host and enclave.
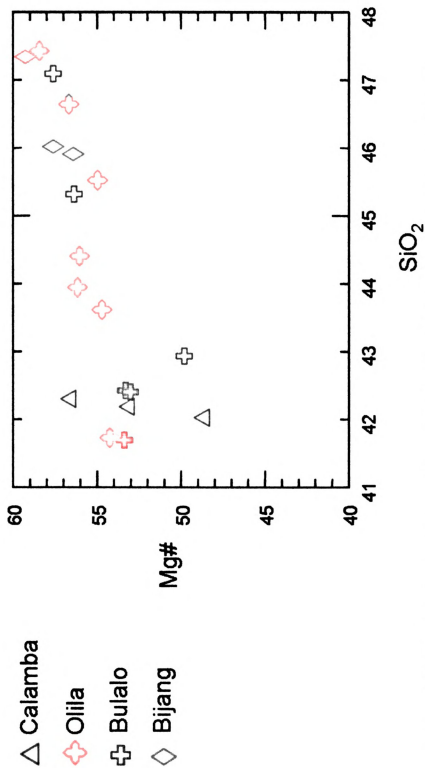
Figure 17b- Magnesium number of amphibole vs. SiO_2 content- there is no correlation between the magnesium number and silica content, or between the enclaves and the host.
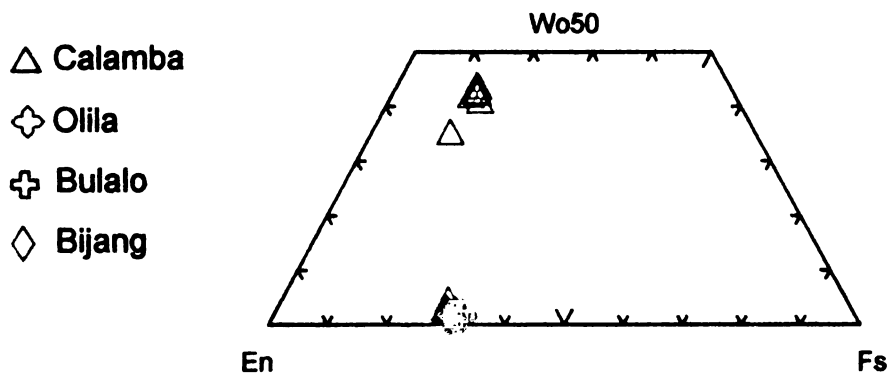
Figure 18a- Pyroxene composition- there is no distinction between the orthopyroxenes of the four domes. The clinopyroxenes of Calamba are chemically similar as well- except for one outlier, 020517-2h- pyx #9.
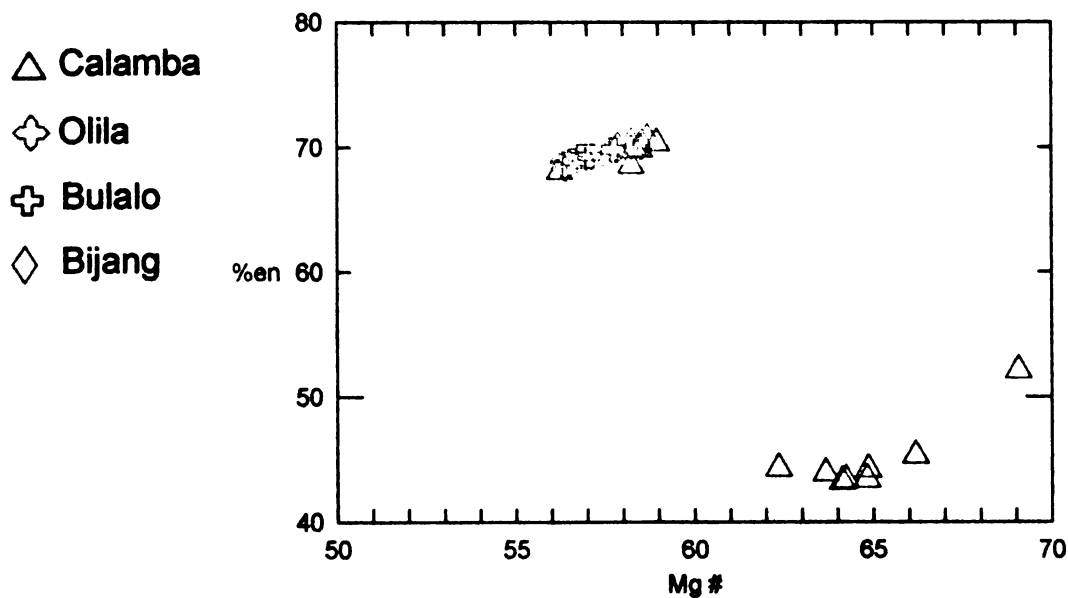
Figure 18b- Plotting enstatite percentage vs. Mg # shows that there is not a wide variation of either in the orthopyroxenes of the four domes, or of the clinopyroxenes of Calamba.

Figure 19- Glass analysis vs. bulk chemical composition. The host glass does not show signs of mingling- the silica values are higher than the bulk composition. The enclave glass from the small enclaves of Olila and Bulalo show some evidence of mingling due to the high silica values.

☆ Matrix Glass-host
★ Matrix Glass-enclave
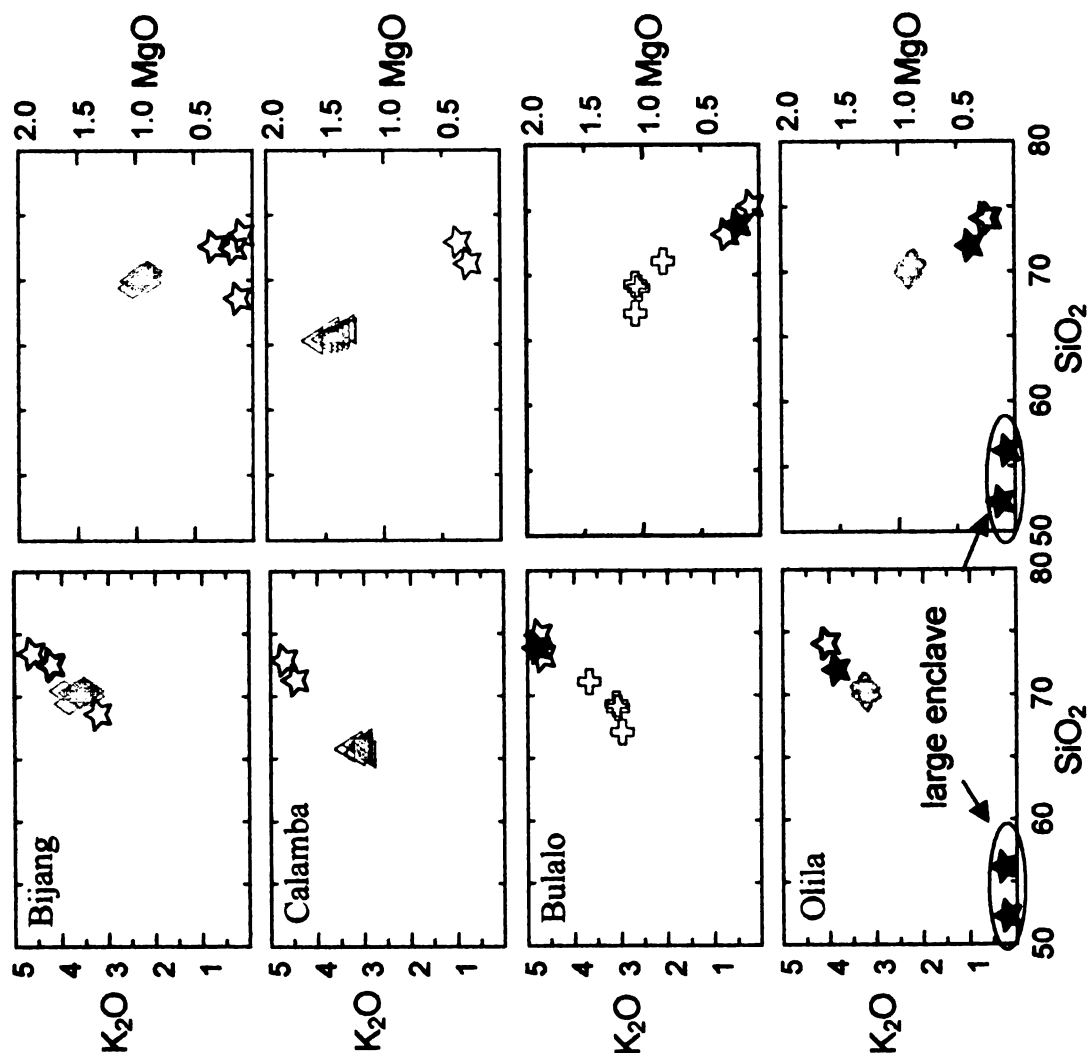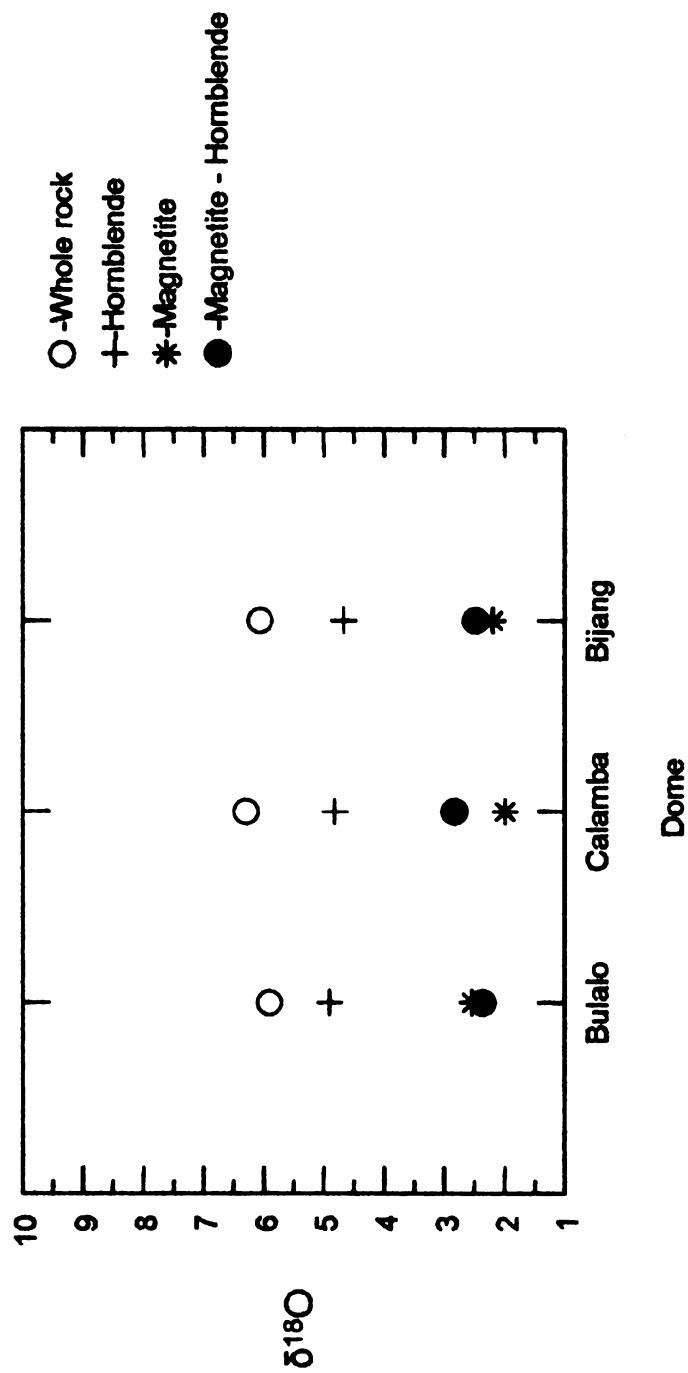
Figure 20- Oxygen isotope values for three domes- $\delta^{18}O$ values for the minerals are very similar, indicating that the values have not been reset. The whole rock values are also very similar, indicating that the three domes originated from a similar source.
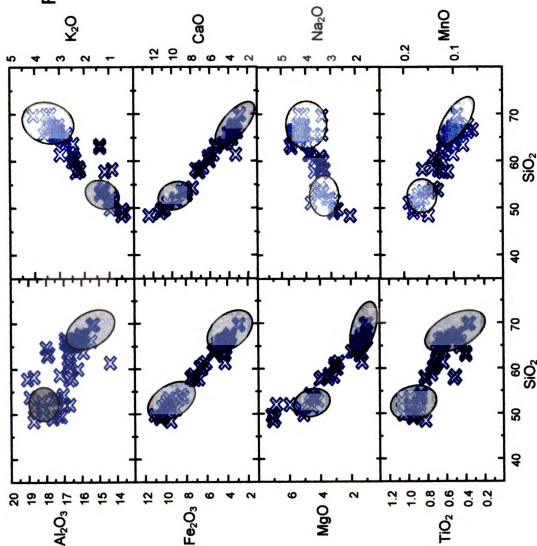
Figure 21a- Plots comparing the chemical composition of the domes with those from Makiling. The dome compositions and the mafic enclaves are represented by the gray areas. It can be seen from this diagram that the dome samples have a major element chemistry that is similar to the Makiling samples.
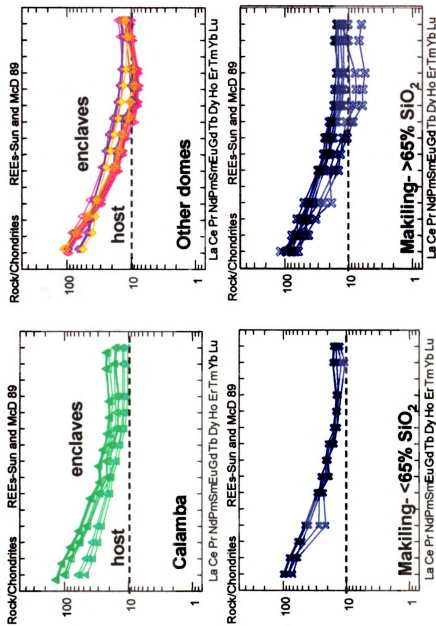
Figure 21b- Diagrams comparing the REE concentrations of the domes and Makiling. The mafic samples are very similar to the mafic enclave compositions of the domes. The silicic samples from Makiling do not show the same depletion in MREEs as those from the domes.
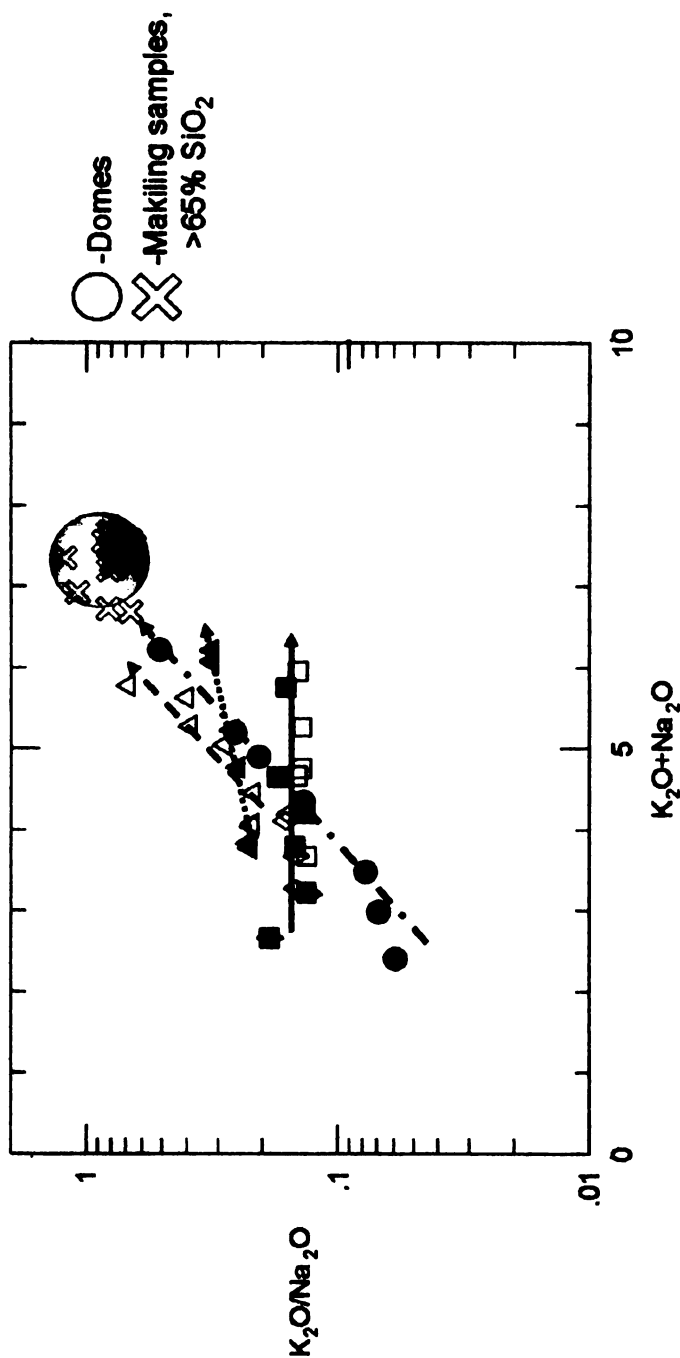
Figure 22- Experimental fractional crystallization trends- solid line represents work of Grove et al (2003) and Muntener et al. (2001) with a basaltic starting composition at varying water pressures and saturation; dotted line represents the trend with an andesitic starting composition (Grove et al., 2003); dashed line represents fractionation trend with andesitic starting composition at shallow pressures (Grove et al., 2003); dotted/dashed line represents fractionation at 1 GPa of a tholeiitic basalt (Villeger, et al., 2004). While the work of Villeger comes close to reproducing the composition of the domes and Makiling, it is through extremely high amounts of fractionation, >90%.
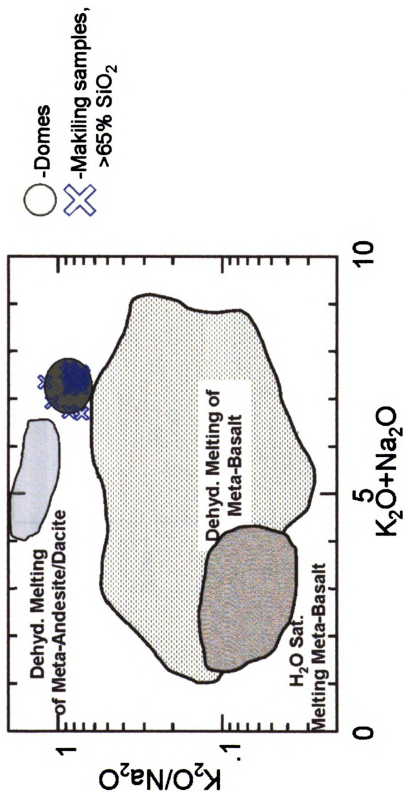
Figure 23- Diagram representing the experimental products of partially melted source rocks of varying composition (Patino-Douce, et al., 1999). The domes do not fall within any fields, but come closest to being reproduced by partial melting of a meta-andesite/dacite.
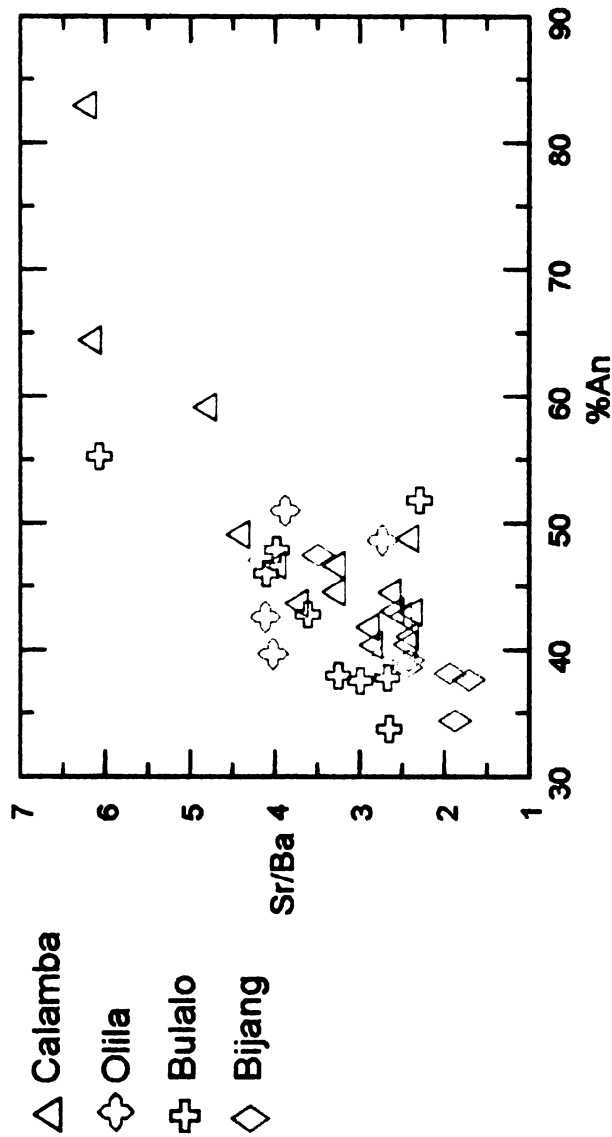
Figure 24- Diagram of Sr/Ba vs %An- There is a general trend of increasing Sr/Ba with increasing %An, up to 50% An. This is indicative of chemistry changes in the plagioclase reflecting changes in melt composition rather than changes in pressure or water content (Browne et al., 2004). The second trend observed is a ratio of 6 for a variety of An compositions. The points found in this second group come from two grains from Calamba and one grain from Bulalo that contain centers with high An. These points most likely represent centers of grains that originated in a more mafic magma. In this case, the change in the major element composition of the plagioclase grains maybe attributed to processes other than compositional changes of the magmas, such as a change in water pressure or temperature (Ginibre et al., 2002).

65
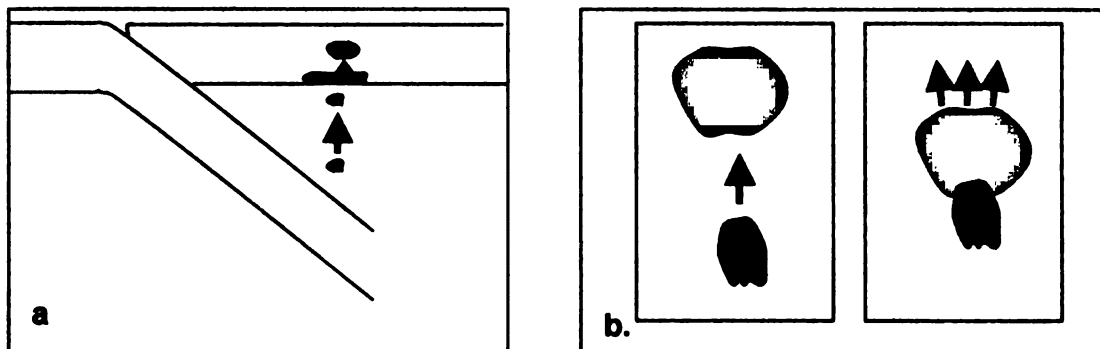
Figure 25- Partial melting and eruption model- a. Dehydration melting of the mantle wedge leads to the formation of a mafic magma. This mafic magma travels through the wedge and encounters a solidified or partially solidified body of calc-alkaline andesite. The heat from the mafic magma partially melts and mobilizes the more siliceous product. This siliceous magma may travel through the crust and erupt at the surface, or it may stall out, requiring an additional influx (b) of hot, mafic magma to cause the eruption. (Not to scale)

APPENDIX 3

TABLES

Table 1- Ages of Selected Domes from the Macolod Corridor

Location	Age (ka)
Trapiche	43 ± 13
Bulalo	15 ± 7
Bijang	66 ± 14

(Source: Heizler, personal communication, 2003)

Table 2- Thermobarometry Results- Calamba

Ilmenite Compositions	MgO	Al₂O₃	SiO₂	CaO	TiO₂	V₂O₃	Cr₂O₃	MnO	FeO	Total
020517-2h (16) il #1	0.98	0.07	0.13	0.01	43.83	0.29	0.06	0.84	51.86	98.08
020517-2d (24) il #1	2.81	0.32	0.05	0.02	39.52	0.30	0.03	0.59	52.19	95.83

Magnetite Compositions	MgO	Al₂O₃	SiO₂	CaO	TiO₂	V₂O₃	Cr₂O₃	MnO	FeO	Total
020517-2h (16) mag #1-1	1.45	2.40	0.46	0.02	9.81	0.43	0.03	0.64	79.75	94.98
020517-2h (16) mag #1-2	1.49	2.34	0.35	0.02	9.63	0.47	0.03	0.64	80.03	95.00
020517-2h (16) mag #1-3	1.40	2.47	0.38	0.01	10.44	0.57	0.06	0.49	78.06	93.87
020517-2h (16) mag #2	0.54	1.76	0.48	0.00	9.41	0.52	0.04	0.71	81.16	94.62
020517-2h (16) mag #3	0.77	2.17	0.17	0.00	11.42	0.40	0.03	0.67	80.57	96.21
020517-2h (16) mag #4	0.80	2.25	0.17	0.03	10.01	0.51	0.07	0.68	81.12	95.65
020517-2h (16) mag #5	0.52	1.96	0.23	0.00	9.88	0.54	0.03	0.74	81.58	95.48

Orthopyroxene Compositions	Na₂O	MgO	Al₂O₃	SiO₂	Cl	K₂O	CaO	TiO₂	Cr₂O₃	MnO	FeO	Total
020517-2h (16) pyx #5	0.04	25.14	0.78	53.92	0.01	0.00	1.14	0.22	0.00	0.85	19.56	101.68
020517-2h (16) pyx #7	0.03	24.18	0.53	51.99	0.00	0.00	1.07	0.16	0.02	1.05	17.33	96.34
020517-2h (16) pyx #10	0.03	24.76	0.53	52.67	0.01	0.01	1.11	0.16	0.02	1.12	17.22	97.66
020517-2h (16) pyx #11	0.02	24.14	0.90	52.31	0.00	0.01	1.17	0.18	0.00	0.87	17.13	96.73

Clinopyroxene Compositions	Na₂O	MgO	Al₂O₃	SiO₂	Cl	K₂O	CaO	TiO₂	Cr₂O₃	MnO	FeO	Total
020517-2h (16) pyx #3	0.36	15.29	1.30	52.05	0.01	0.00	21.28	0.34	0.02	0.48	8.29	99.44
020517-2h (16) pyx #2	0.41	15.54	1.32	52.76	0.02	0.01	21.66	0.33	0.00	0.55	8.69	101.29
020517-2h (16) pyx #1	0.40	15.68	1.48	52.53	0.02	0.03	21.71	0.40	0.03	0.50	8.73	101.50
020517-2h (16) pyx #4	0.40	16.03	1.94	52.22	0.00	0.00	20.52	0.56	0.03	0.61	9.68	101.99
020517-2d (24) pyx #6	0.40	15.65	1.37	52.24	0.00	0.00	20.91	0.37	0.00	0.52	8.93	100.41
020517-2d (24) pyx #7	0.33	15.60	1.34	52.21	0.00	0.01	20.86	0.39	0.01	0.53	8.45	99.78
020517-2h (16) pyx #9	0.24	17.48	2.25	52.89	0.01	0.03	16.26	0.31	0.00	0.36	7.83	97.72
020517-2h (16) pyx #12	0.37	15.21	1.14	51.33	0.00	0.00	19.50	0.31	0.01	0.53	7.77	96.19

Table 2 (cont'd)

Ilmenite/Magnetite Pairs	Temp (K)	Uncertainty	fO$_2$	Temp (°C)	Uncertainty
ii #1 (24) + mag #6	1125	137	-11.26	852	103.75
ii #1 (24) + mag #7	1102	174	-11.52	829	130.89
ii #1 (16) + mag #7	1098	86	-12.31	825	64.62
ii #1 (16) + mag #6	1103	101	-12.24	830	76.00
ii #1 (16) + mag #1	1091	158	-12.34	818	118.46
ii #1 (16) + mag #5*	1127	85	-11.92	854	64.41
Pyroxene Pairs					
cpx #9 + opx #10	1249	89		976	69.55
cpx #12 + opx #10*	1229	19		956	14.78
cpx #12 + opx #7	1219	24		946	18.63
Both systems- best match					
ii #1 (16) + mag #5; cpx #12 + opx #10	856	88	-15.33	583	59.93
	1022	65	-12.00	749	47.64

70

Table 3- Oxygen Data

	Bulalo	Calamba	Bijang
Whole Rock	5.90	6.29	6.06
Magnetite	2.36 ± .08	2.83 (1 analysis)	2.48 ± .12
Hornblende	4.90 ± .03	4.82 ± .14	4.67 ± .06
Difference	2.54	1.99	2.19

Table 4a- Bulk Chemical Analyses- Major Elements*

Sample	Dome	SiO_2	TiO_2	Al_2O_3	Fe_2O_3	MnO	MgO	CaO	Na_2O	K_2O	P_2O_5	Totals
020518-1TAV-b	Bijang	69.43	0.39	15.53	3.14	0.08	1.03	2.98	3.46	3.85	0.1	100
020518-1c	Bijang	69.83	0.4	15.23	3.21	0.08	0.91	2.78	3.84	3.61	0.1	100
020518-1h	Bijang	69.94	0.41	15.03	3.32	0.09	1.01	2.78	3.71	3.61	0.1	100
020518-1f	Bijang	70.02	0.39	15.32	2.99	0.08	0.95	2.75	3.8	3.6	0.1	100
020518-1d	Bijang	70.06	0.41	15.04	3.29	0.08	1	2.81	3.8	3.41	0.1	100
020518-1TAV-a	Bijang	70.34	0.38	15.14	3	0.08	0.93	2.75	3.69	3.58	0.1	100
121502-4A	Bijang	70.34	0.4	14.94	3.17	0.08	0.93	2.65	3.62	3.76	0.11	100
020518-1b	Bijang	70.37	0.38	15.06	2.97	0.08	0.91	2.74	3.73	3.65	0.1	100
020518-1e	Bijang	70.46	0.39	14.99	3.03	0.08	0.92	2.7	3.9	3.42	0.1	100
020518-1g	Bijang	70.48	0.38	14.88	2.98	0.08	0.91	2.68	3.54	3.95	0.1	100
121502-4B	Bijang	70.53	0.38	15.01	2.84	0.08	0.94	2.74	3.75	3.62	0.11	100
020518-1a	Bijang	70.6	0.38	14.88	3	0.08	0.9	2.79	3.74	3.53	0.1	100
020518-1TAV-c	Bijang	70.72	0.37	15.03	2.82	0.08	0.9	2.71	3.72	3.53	0.1	100
020522-51TAV	Bulalo	50.93	1.08	18.2	10.89	0.18	4.41	9.88	3.17	1.04	0.21	100
020522-51tavE1	Bulalo	51.86	1.05	18.15	10.43	0.18	4.28	9.48	3.18	1.17	0.21	100
020522-51tavE2	Bulalo	52.16	1.06	17.99	10.49	0.18	4.1	9.45	3.18	1.18	0.21	100
020522-1	Bulalo	67.09	0.45	17.42	3.43	0.1	1.06	3.42	3.92	2.97	0.12	100
121502-1A	Bulalo	69.02	0.4	15.73	3.2	0.1	1.03	3	4.35	3.05	0.12	100
121502-1B	Bulalo	69.33	0.4	15.46	3.13	0.1	1.06	2.97	4.34	3.09	0.13	100
020522-50TAV	Bulalo	71.12	0.38	14.65	2.89	0.09	0.82	2.44	3.83	3.67	0.11	100
020517-2c	Calamba	51.61	0.9	18.22	9.22	0.15	5.31	10.51	3.04	0.91	0.14	100
020517-2e	Calamba	53.27	0.99	17.95	9.22	0.16	4.5	9.13	3.36	1.25	0.16	100
020517-2a	Calamba	54.2	0.82	18.42	7.98	0.15	4.22	9.1	3.43	1.51	0.16	100
020517-2m	Calamba	65.34	0.71	16.07	4.96	0.11	1.58	3.93	4.22	2.9	0.17	100
121502-3A	Calamba	65.45	0.69	16.31	4.58	0.11	1.5	3.66	4.39	3.13	0.16	100
020517-2d*	Calamba	65.49	0.69	16.18	4.53	0.11	1.45	3.81	4.43	3.13	0.16	100
020517-2i	Calamba	65.56	0.7	16.13	4.81	0.11	1.41	3.85	4.29	2.97	0.16	100
020517-2g	Calamba	65.65	0.65	16.49	4.42	0.1	1.36	3.82	4.36	2.99	0.16	100

Table 4a (cont'd)

Sample	Dome	SiO2	TiO2	Al2O3	Fe2O3	MnO	MgO	CaO	Na2O	K2O	P2O5	Totals
020517-2i	Calamba	65.56	0.7	16.13	4.81	0.11	1.41	3.85	4.29	2.97	0.16	100
020517-2g	Calamba	65.65	0.65	16.49	4.42	0.1	1.36	3.82	4.36	2.99	0.16	100
020517-2l	Calamba	65.8	0.66	16.15	4.6	0.11	1.45	3.8	3.94	3.34	0.15	100
020517-2b	Calamba	65.9	0.66	16.23	4.46	0.1	1.35	3.81	4.33	3.01	0.16	100
020517-2k	Calamba	65.92	0.64	16.3	4.41	0.1	1.39	3.79	4.32	2.97	0.16	100
020517-2f	Calamba	66.1	0.67	16.13	4.51	0.1	1.29	3.68	4.31	3.04	0.17	100
020517-2h	Calamba	66.3	0.64	16.1	4.37	0.1	1.31	3.82	4.23	2.98	0.16	100
020522-52TAV	Olila	53.52	0.87	17.98	9.47	0.17	4.44	9	3.03	1.31	0.21	100
020522-56TAV	Olila	69.84	0.38	15.4	2.93	0.09	0.91	2.95	4.16	3.19	0.13	100
020522-54TAV	Olila	69.97	0.4	15.39	2.93	0.09	0.92	2.73	4.21	3.24	0.12	100
020522-53TAV	Olila	70.48	0.38	15.09	2.9	0.09	0.89	2.8	4.03	3.22	0.13	100
020522-55TAV	Olila	70.59	0.38	15.04	2.84	0.09	0.87	2.68	4.13	3.28	0.11	100

* All values normalized
  to 100

73

Table 4b- Bulk Chemical Analyses- Trace Elements

Sample	Dome	Cr	Ni	Cu	Zn	Rb	Sr	Zr	V-ICPMS	Cr-ICPMS	Y
020518-1TAV-b	Bijang	-30.1	-3.2	4.4	37.2	89.6	326.9	164	71.37	5.81	13.15
020518-1c	Bijang	-27.5	-2	10.4	36.9	94.1	309.9	161.3	78.89	6.16	13.34
020518-1h	Bijang	-26.1	-0.1	6.1	39	91.7	304.8	162.4	81.04	5.81	13.39
020518-1f	Bijang	-36	2	-2	30	89	315	170	68.12	6.9	12.49
020518-1d	Bijang	-27.3	-5.4	10.9	37.6	90.9	308.7	161.1	73.3	5.4	13.68
020518-1TAV-a	Bijang	-28	3	-4	31	93	309	168	69.17	7.3	12.21
121502-4A	Bijang					107	304	167	75.69	6.99	12.47
020518-1b	Bijang	-34.8	-1.8	8	34.8	97.2	306.1	163.1	66.09	4.85	12.67
020518-1e	Bijang	-31	1	-2	31	89	307	167	68.4	7.43	12.24
020518-1g	Bijang	-22.5	-2.8	5.3	34.5	95.7	297.2	158.6	64.66	5.13	12.48
121502-4B	Bijang					99	310	163	63.73	6.49	12.79
020518-1a	Bijang	-31.3	2.4	-1.4	31.2	94.6	306.5	159.7	70.05	5.67	12.66
020518-1TAV-c	Bijang	-31.4	-0.3	2.4	32.1	95.6	301.7	162.9	60.46	6.38	12.66
020522-51TAV	Bulalo	-10.7	4.2	96.1	70.1	23.4	596.7	85.62	355.3	4.87	22.68
020522-51tavE1	Bulalo	-16	3.9	74.9	70.1	30.6	584	89.4	351.62	5.03	21.96
020522-51tavE2	Bulalo	-17.4	2.8	81.7	68.5	27.6	585.9	86	348.12	6.33	23.01
020522-1	Bulalo	-12	-18	1	36	74	381	171.32	74.23	5.94	15.06
121502-1A	Bulalo					81	339	170	79.06	8.58	12.76
121502-1B	Bulalo					85	332	168	65.43	6.54	13.77
020522-50TAV	Bulalo	-32.1	0.3	1.9	32.3	90.3	269.2	181.55	54.24	5.11	13.15
020517-2c	Calamba	54	19	50	65	20	535	61	277.02	64.02	17.92
020517-2e	Calamba	-1	3	63	71	26	523	80	277.4	16.76	20.92
020517-2a	Calamba	23	8	33	58	36	522	83	244.61	45.2	19.02
020517-2m	Calamba	-27.8	-1.7	20.4	47.1	70.6	343.1	188.2	132.15	5.56	23.67
121502-3A	Calamba					82	338	197	112.12	6.59	26.04
020517-2d*	Calamba	-20	0	14	45	73	314	175	97.32	5.95	23.86
020517-2i	Calamba	-27.1	-0.7	17.5	47.8	73.4	341.6	192	120.96	5.93	23.43

74

Table 4b (cont'd)

Sample	Dome	Cr	Ni	Cu	Zn	Rb	Sr	Zr	V-ICPMS	Cr-ICPMS	Y
020517-2g	Calamba	-35	1	28	42	72	352	193	104.75	5.95	24.02
020517-2l	Calamba	-25.7	1.1	11.8	45.5	77.8	337	193	111.76	6.34	23.96
020517-2b	Calamba	-31	1	19	47	74	341	185	102.78	5.65	25.47
020517-2k	Calamba	-27.9	1.1	30.8	41.9	75.7	345.2	195.4	110.44	6.04	23.75
020517-2f	Calamba	-31	1	34	41	69	335	196	103.37	5.32	26.04
020517-2h	Calamba	-25.9	1	12	39.6	74.8	343.5	190.9	104.63	5.16	22.88
020522-52TAV	Olila	-2	8.3	40.6	64.9	31.2	504	87.3	286.54	3.3	19.87
020522-56TAV	Olila	-42	-2.6	11	40.4	80.1	322.9	165	60.1	5.62	14.48
020522-54TAV	Olila	-36.7	1	1.5	37	86.2	306.8	183.2	54.37	5.04	13.35
020522-53TAV	Olila	-27.9	1.3	5	37.1	85.6	310.4	176.65	54.2	4.83	13.56
020522-55TAV	Olila	-44.5	-2.2	10	42.5	86.1	295.4	173	56.78	5.1	12.54

75

Table 4b (cont'd)

Sample	Nb	Ba	La	Ce	Pr	Nd	Sm	Eu	Gd	Tb	Dy
020518-1TAV-b	8.58	762.14	22.93	41.54	4.25	14.8	2.79	0.82	2.74	0.41	2.09
020518-1c	10.06	781.56	23.03	42.78	4.27	13.96	2.78	0.83	2.79	0.4	2.01
020518-1h	9.09	776.13	23.24	42.51	4.26	14.44	2.91	0.84	2.8	0.41	2.12
020518-1f	8.87	765.93	22.12	40.96	4.14	13.48	2.41	0.81	2.53	0.36	2.03
020518-1d	8.96	775.79	22.88	41.05	4.28	14.36	2.86	0.85	2.8	0.4	2.25
020518-1TAV-a	8.82	778.67	22.32	40.96	4.06	13.64	2.67	0.82	2.47	0.33	2.05
121502-4A	9.12	817.18	22.32	44.92	4.17	13.44	2.52	0.79	2.62	0.43	2.04
020518-1b	8.82	792.46	22.25	40.99	3.97	13.06	2.46	0.78	2.58	0.39	1.98
020518-1e	8.42	766.73	21.91	39.68	3.88	13.66	2.45	0.79	2.44	0.36	2.06
020518-1g	8.75	775.6	22.48	41	4.02	13.2	2.46	0.75	2.57	0.38	1.9
121502-4B	8.72	813.81	22.47	44.85	4.25	13.81	2.64	0.84	2.7	0.47	2.14
020518-1a	8.66	780.12	22.65	41.53	4.13	13.36	2.69	0.74	2.55	0.39	2.05
020518-1TAV-c	8.36	797.49	22.87	41.87	4.2	13.81	2.54	0.79	2.45	0.36	1.92
020522-51TAV	3.06	324.55	14.61	27.41	3.81	17.21	4	1.36	4.11	0.65	3.91
020522-51tavE1	3.13	317.39	14.3	26.88	3.71	16.83	3.91	1.33	4.05	0.64	3.85
020522-51tavE2	3.59	353.1	15.24	28.49	3.99	17.28	3.98	1.39	4.42	0.69	4.02
020522-1	8.52	789	21.52	42.71	4.25	14.69	2.76	0.86	2.67	0.43	2.14
121502-1A	10.08	843.47	22.9	47.03	4.41	14.25	2.78	1.02	2.82	0.51	2.14
121502-1B	8.16	841.15	23.19	44.59	4.31	14.73	2.89	0.93	2.92	0.46	2.49
020522-50TAV	7.74	826.33	23.87	41.12	4.22	14.21	2.45	0.78	2.59	0.35	2.35
020517-2c	4.31	262.86	10.67	21.55	2.76	11.82	2.87	1.04	3.06	0.49	2.88
020517-2e	5.25	303.5	13.33	25.22	3.2	13.58	3.2	1.11	3.35	0.54	3.24
020517-2a	5.11	357.34	14.78	28.69	3.55	14.64	3.39	1.2	3.41	0.53	3.08
020517-2m	10.1	648.88	23.88	49.23	5.42	20.19	4.29	1.26	4.35	0.65	3.76
121502-3A	10.47	668.34	23.27	49.61	5.57	21.28	4.56	1.25	4.63	0.74	4.15
020517-2d*	9.01	622.03	21.85	46.03	5.19	19.35	4.06	1.1	4.04	0.63	3.64
020517-2i	10.6	667.37	24.1	50.16	5.78	21.41	4.57	1.27	4.59	0.69	3.78

Table 4b (cont'd)

Sample	Nb	Ba	La	Ce	Pr	Nd	Sm	Eu	Gd	Tb	Dy
020517-2g	10.34	672.22	24.16	49.32	5.56	21.18	4.47	1.25	4.45	0.67	4.29
020517-2l	10.55	671.07	24.97	52.16	5.97	21.78	4.53	1.23	4.7	0.71	3.92
020517-2b	9.28	650.48	24.04	49.06	5.59	20.93	4.5	1.23	4.35	0.7	3.89
020517-2k	10.73	681.76	24.89	52.22	5.77	20.89	4.73	1.28	4.55	0.7	3.87
020517-2f	9.54	665.8	23.95	50	5.75	21.72	4.66	1.24	4.51	0.73	3.97
020517-2h	10.32	670.33	23.25	49.36	5.54	20.28	4.26	1.16	4.34	0.66	3.56
020522-52TAV	2.97	291.2	12.89	23.74	3.3	14.98	3.63	1.17	3.65	0.57	3.52
020522-56TAV	8.83	885.26	25.84	45.37	4.58	15.79	2.85	0.91	2.82	0.41	2.62
020522-54TAV	7.79	794.31	23.56	42.01	4.29	15.23	2.62	0.86	2.68	0.39	2.51
020522-53TAV	7.52	804.69	23.84	42.45	4.36	15.42	2.66	0.87	2.69	0.4	2.52
020522-55TAV	7.89	801.52	22.97	40.9	4.05	13.94	2.46	0.81	2.61	0.35	2.42

77

Table 4b (cont'd)

Sample	Ho	Er	Yb	Lu	Hf	Ta	Pb	Th
020518-1TAV-b	0.47	1.42	1.87	0.26	4.08	0.66	36.5	16.5
020518-1c	0.47	1.46	1.73	0.28	3.86	0.66	35.4	15.36
020518-1h	0.48	1.48	1.76	0.27	4.1	0.66	35.95	16.05
020518-1f	0.45	1.37	1.65	0.26	4.12	0.74	23.62	15.17
020518-1d	0.5	1.49	1.87	0.28	4.21	0.67	34.38	15.91
020518-1TAV-a	0.44	1.27	1.6	0.27	3.9	0.72	21.65	14.14
121502-4A	0.49	1.49	1.64	0.24	3.83	0.67	33.3	15.93
020518-1b	0.44	1.25	1.64	0.24	3.94	0.66	38.03	15.92
020518-1e	0.46	1.28	1.6	0.27	4.11	0.74	22.72	14.79
020518-1g	0.45	1.3	1.64	0.25	3.93	0.66	35.14	15.71
121502-4B	0.5	1.49	1.71	0.25	3.63	0.68	33.21	15.52
020518-1a	0.41	1.26	1.76	0.27	3.84	0.64	35.2	15.31
020518-1TAV-c	0.42	1.31	1.71	0.24	3.95	0.61	35.95	15.78
020522-51TAV	0.83	2.24	2.19	0.35	2.3	0.23	4.31	3.8
020522-51tavE1	0.81	2.2	2.16	0.34	2.34	0.22	5.7	3.81
020522-51tavE2	0.83	2.27	2.24	0.36	2.65	0.27	6.49	4.54
020522-1	0.47	1.38	1.86	0.28	3.67	0.56	26.02	12.47
121502-1A	0.54	1.49	1.73	0.27	3.49	0.71	33.93	14.15
121502-1B	0.56	1.69	1.96	0.3	3.98	0.66	33.88	16.69
020522-50TAV	0.43	1.45	1.7	0.32	4.42	0.81	24.43	15.67
020517-2c	0.61	1.69	1.76	0.26	1.61	0.24	6.48	2.95
020517-2e	0.7	2.05	2.1	0.32	2.17	0.3	7.62	3.96
020517-2a	0.67	1.9	2	0.3	2.1	0.3	8.29	4.55
020517-2m	0.82	2.32	2.69	0.4	4.19	0.56	15.55	10.46
121502-3A	0.88	2.67	2.84	0.41	4.49	0.61	20.03	11.01
020517-2d*	0.81	2.38	2.75	0.38	4.21	0.5	15.43	9.6
020517-2i	0.83	2.39	2.8	0.42	4.66	0.6	18.26	10.97

Table 4b (cont'd)

Sample	Ho	Er	Yb	Lu	Hf	Ta	Pb	Th
020517-2g	0.87	2.6	2.9	0.44	4.84	0.68	12.56	11.44
020517-2l	0.85	2.46	2.88	0.44	4.91	0.63	21.51	11.64
020517-2b	0.84	2.5	2.89	0.43	4.45	0.52	11.88	10.31
020517-2k	0.84	2.48	2.83	0.41	4.55	0.61	21.01	11.25
020517-2f	0.88	2.5	2.95	0.42	4.55	0.52	13.63	10.13
020517-2h	0.81	2.2	2.53	0.39	4.43	0.56	17.44	11.02
020522-52TAV	0.72	1.92	1.87	0.3	2.22	0.22	6.63	3.74
020522-56TAV	0.52	1.65	1.95	0.35	4.56	0.78	25.24	16.46
020522-54TAV	0.48	1.49	1.77	0.31	4.17	0.67	21.66	14.83
020522-53TAV	0.48	1.5	1.78	0.3	4.07	0.68	22.55	14.64
020522-55TAV	0.45	1.44	1.61	0.29	4.32	0.67	22.78	14.48

Table 5- Plagioclase Major Element Analyses

Well-zoned Plagioclase

Sample	Dome	Na2O	MgO	Al2O3	SiO2	K2O	CaO	TiO2	BaO	FeO	SrO	Total	% An
020518-1c (15) plag #2-core	Bjiang	6.77	0.04	25.60	58.04	0.47	8.07	0.01	0.27	-0.11	0.02	99.28	38.65
020518-1c (15) plag #2-mid1	Bjiang	6.74	0.02	25.65	57.01	0.47	8.22	0.01	0.31	-0.07	0.10	98.51	39.19
020518-1c (15) plag #2-mid2	Bjiang	6.82	0.03	25.87	58.93	0.48	7.80	0.04	0.30	0.02	-0.04	100.29	37.65
020518-1c (15) plag #2-rim	Bjiang	6.66	0.02	25.69	58.09	0.47	8.00	0.01	0.32	-0.08	0.04	99.48	38.14
020518-1c (15) plag #4 core	Bjiang	5.96	0.02	27.69	56.38	0.31	10.08	0.02	0.23	0.03	0.12	100.84	47.48
020518-1c (15) plag #4 mid	Bjiang	7.21	0.03	25.21	59.77	0.58	7.21	-0.01	0.25	-0.09	0.06	100.32	34.41
020518-1c (15) plag #4 rim	Bjiang	6.87	0.03	25.89	58.08	0.46	7.93	0.02	0.32	-0.07	-0.01	99.61	37.90
020518-1f (19) plag #1 core	Bjiang	5.78	0.03	26.28	53.02	0.29	8.18	0.00	0.05	0.27	0.00	93.89	43.12
020518-1f (19) plag #1rim	Bjiang	6.75	0.03	24.93	55.41	0.46	6.50	0.01	0.01	0.34	0.00	94.44	33.73
020518-1f (19) plag #3 core	Bjiang	6.33	0.01	24.94	56.70	0.45	6.97	0.00	0.07	0.28	0.12	95.87	36.76
020518-1f (19) plag #3 mid	Bjiang	6.69	0.01	24.86	57.08	0.49	6.51	0.00	0.00	0.32	0.05	96.01	33.91
020518-1f (19) plag #3 rim	Bjiang	5.88	0.01	25.57	55.73	0.39	7.75	0.02	0.11	0.24	0.00	95.71	41.12
020522-51 (94) plag #2-core	Bulalo	4.87	0.02	28.97	53.23	0.19	11.16	0.04	0.34	0.00	0.02	99.83	55.27
020522-51 (94) plag #2-rim	Bulalo	5.22	0.02	28.94	54.41	0.24	10.47	0.03	0.39	0.00	0.00	99.69	51.82
020522-51 (94) plag #3-core	Bulalo	6.18	0.02	27.13	56.01	0.34	9.00	0.00	0.29	0.10	0.01	99.09	43.71
020522-51 (94) plag #3-mid1	Bulalo	5.80	0.01	27.97	54.75	0.27	9.73	0.00	0.32	0.00	0.09	98.95	47.35
020522-51 (94) plag #3-mid2	Bulalo	6.00	0.01	27.76	55.23	0.29	9.89	0.03	0.32	0.04	0.00	99.56	46.87
020522-51 (94) plag #3-rim	Bulalo	6.79	0.01	25.97	57.61	0.44	7.60	0.00	0.33	0.00	0.04	98.79	37.24
020522-51 (94) plag #4-core	Bulalo	5.84	0.01	27.83	55.42	0.25	9.98	0.02	0.35	0.06	0.12	99.87	47.88
020522-51 (94) plag #4-rim	Bulalo	6.47	0.01	26.71	56.76	0.34	8.49	0.00	0.33	0.00	0.01	99.11	41.19
020522-51 (94) plag #4-rim	Bulalo	7.41	0.02	24.94	59.05	0.52	6.81	0.01	0.24	0.02	0.07	99.10	32.70
020522-51 (94) plag #6 core-a	Bulalo	6.01	0.03	26.93	55.89	0.30	9.58	0.00	0.33	0.03	0.07	99.17	46.02
020522-51 (94) plag #6 mid	Bulalo	7.28	0.02	25.06	59.60	0.48	7.00	0.00	0.27	0.02	0.10	99.81	33.76
020522-51 (94) plag #6 rim	Bulalo	7.24	0.02	25.12	59.47	0.51	7.01	-0.01	0.22	-0.02	-0.01	99.59	33.81
020517-2d (24) plag #1 core	Calamba	6.16	0.04	26.91	56.71	0.38	9.32	0.03	0.05	0.40	0.04	100.02	44.56
020517-2d (24) plag #1 rim	Calamba	6.54	0.04	26.06	57.29	0.46	8.39	0.03	0.07	0.33	0.04	99.26	40.37
020517-2d (24) plag #3 core	Calamba	1.88	0.03	33.52	46.50	0.05	16.81	0.04	0.07	0.55	0.06	99.52	82.94

Table 5 (cont'd)

Sample	Dome	Na$_2$O	MgO	Al$_2$O$_3$	SiO$_2$	K$_2$O	CaO	TiO$_2$	BaO	FeO	SrO	Total	% An
020517-2d (24) plag #3 mid	Calamba	4.50	0.03	29.18	52.32	0.20	12.12	0.05	0.00	0.48	0.06	98.94	59.15
020517-2d (24) plag #3 rim	Calamba	6.48	0.06	25.89	57.34	0.45	8.32	0.02	0.03	0.40	0.00	98.98	40.42
020517-2d (24) plag #4 core	Calamba	6.02	0.04	27.17	55.93	0.38	9.64	0.03	0.02	0.39	0.08	99.69	45.95
020517-2d (24) plag #4 rim	Calamba	6.15	0.04	24.31	56.98	0.41	8.74	0.02	0.07	0.41	0.00	97.14	42.94
020517-2d (24) plag #5 core	Calamba	5.61	0.04	27.97	55.32	0.33	10.18	0.04	0.00	0.42	0.00	99.91	49.08
020517-2d (24) plag #5 mid	Calamba	6.38	0.04	26.60	56.97	0.45	8.67	0.05	0.06	0.40	0.00	99.61	41.80
020517-2d (24) plag #5 rim	Calamba	6.56	0.03	26.38	57.91	0.49	8.43	0.03	0.01	0.34	0.00	100.15	40.38
020517-2h (16) plag #1 core	Calamba	5.89	0.04	27.23	55.61	0.39	9.69	0.03	0.06	0.45	0.00	99.38	46.55
020517-2h (16) plag #1 mid	Calamba	5.80	0.04	27.28	55.48	0.35	9.77	0.02	0.01	0.43	0.00	99.17	47.24
020517-2h (16) plag #1 rim	Calamba	6.19	0.05	26.68	56.49	0.42	9.01	0.03	0.00	0.42	0.00	99.29	43.49
020517-2h (16) plag #2 core	Calamba	5.73	0.03	27.50	55.39	0.36	10.07	0.00	0.07	0.44	0.12	99.69	48.27
020517-2h (16) plag #2 rim	Calamba	6.94	0.03	25.62	58.44	0.52	7.81	0.06	0.00	0.40	0.03	99.84	37.22
020517-2h (16) plag #3 core	Calamba	5.83	0.03	27.26	55.63	0.34	9.75	0.02	0.05	0.48	0.00	99.41	47.08
020517-2h (16) plag #3 mid	Calamba	5.79	0.03	27.38	55.78	0.35	9.82	0.03	0.01	0.39	0.00	99.58	47.43
020517-2h (16) plag #3 rim	Calamba	6.69	0.04	25.91	57.61	0.51	8.29	0.02	0.15	0.41	0.00	99.63	39.47
020517-2m (31) plag #1 core	Calamba	5.89	0.05	27.29	55.58	0.40	9.73	0.01	0.03	0.42	0.00	99.40	46.66
020517-2m (31) plag #1 mid	Calamba	6.28	0.04	26.81	56.75	0.39	9.17	0.01	0.02	0.43	0.00	99.93	43.66
020517-2m (31) plag #1 rim	Calamba	6.03	0.03	26.58	56.11	0.54	9.27	0.04	0.02	0.43	0.00	99.06	44.51
020517-2m (31) plag #3 core	Calamba	3.91	0.03	30.56	50.91	0.18	13.36	0.04	0.04	0.53	0.00	99.55	64.71
020517-2m (31) plag #3 mid1	Calamba	5.84	0.04	27.79	55.59	0.34	9.60	0.03	0.00	0.45	0.05	99.73	46.68
020517-2m (31) plag #3 mid2	Calamba	5.64	0.05	28.02	54.48	0.33	10.10	0.01	0.06	0.45	0.07	99.20	48.79
020517-2m (31) plag #3 rim	Calamba	6.33	0.03	26.75	56.69	0.46	8.92	0.01	0.05	0.44	0.00	99.67	42.63
020517-2m (31) plag #4 core	Calamba	6.08	0.04	27.18	57.01	0.63	8.85	0.03	0.00	0.49	0.00	100.30	42.97
020517-2m (31) plag #4 mid	Calamba	6.45	0.04	26.16	57.11	0.51	8.56	0.04	0.01	0.43	0.00	99.31	41.07
020517-2m (31) plag #4 rim	Calamba	6.14	0.03	26.28	56.28	0.57	8.91	0.04	0.00	0.46	0.00	98.72	43.06
020522-53 (100) plag #1 core	Oilia	6.42	0.01	26.39	56.76	0.39	8.32	0.00	0.26	0.00	0.07	98.62	40.77
020522-53 (100) plag #1 mid1	Oilia	5.96	0.03	26.92	55.91	0.28	9.22	0.01	0.28	0.00	0.01	98.61	45.36
020522-53 (100) plag #1 mid2	Oilia	6.23	0.01	26.76	56.70	0.36	8.87	0.02	0.35	0.05	0.01	99.35	43.15

81

Table 5 (cont'd)

Sample	Dome	Na2O	MgO	Al2O3	SiO2	K2O	CaO	TiO2	BaO	FeO	SrO	Total	% An
020522-53 (100) plag #1 rim	Ollia	5.49	0.02	27.71	54.58	0.30	9.97	0.01	0.38	0.00	0.00	98.44	49.22
020522-53 (100) plag #2 core	Ollia	5.64	0.02	27.75	54.77	0.25	10.17	0.02	0.41	0.00	0.00	99.02	49.19
020522-53 (100) plag #2 mid	Ollia	7.19	0.00	25.15	59.39	0.50	7.22	0.04	0.31	0.00	0.00	99.79	34.66
020522-53 (100) plag #2 nm	Ollia	6.80	0.03	25.91	57.71	0.42	7.78	0.03	0.27	0.00	0.05	99.01	37.77
Non-zoned plagioclase													
020518-1c (15) plag#1-core	Bijang	6.857	0.033	25.785	57.905	0.488	7.799	0.021	0.259	-0.073	0.063	99.21	37.52
020518-1c (15) plag#1-mid	Bijang	7.486	0.026	24.514	59.704	0.61	6.764	0.038	0.306	-0.085	0.113	99.56	32.15
020522-51 (94) plag #1-core	Bulalo	5.766	0.016	27.765	55.235	0.231	9.628	0.026	0.33	0.047	0.126	99.171	47.34
020522-51 (94) plag #1-rim	Bulalo	6.119	0.014	27.106	56.258	0.317	9.111	0.01	0.341	0	0	99.275	44.31
020522-53 (100) plag #3-1	Ollia	5.792	0.018	27.372	55.124	0.305	9.855	0.02	0.289	0	0.03	98.805	47.61
020522-53 (100) plag #3-2	Ollia	5.909	0.017	27.618	55.209	0.304	9.674	0.027	0.323	0	0.078	99.159	46.67
020522-53 (100) plag #3-3	Ollia	4.977	0.005	29.316	53.012	0.209	11.296	0.014	0.342	0.036	0	99.206	54.96
020522-53 (100) plag #3-4	Ollia	6.648	0.025	25.88	57.506	0.424	8.017	0	0.27	0.012	0.012	98.793	39.01
020522-53 (100) plag #6-core	Ollia	5.51	0.045	26.882	54.612	0.28	9.835	0.038	0.517	0.195	-0.03	97.916	48.83
020522-53 (100) plag #6-rim	Ollia	6.645	0.009	25.517	58.012	0.39	8.054	0.015	0.235	0.092	-0.01	98.969	39.21
020522-53 (100) plag #6-core2	Ollia	5.488	0.048	28.066	55.015	0.268	10.658	0.036	0.415	-0.023	-0.01	99.992	50.98
020522-53 (100) plag #7-rim	Ollia	5.193	0.033	27.689	53.804	0.262	10.928	0.018	0.395	0.11	-0.01	98.431	39.21
020522-53 (100) plag #7-core	Ollia	5.54	0.024	27.179	55.014	0.285	9.93	0.022	0.436	0.09	0.006	98.525	48.93
020522-53 (100) plag #8-core	Ollia	5.969	0.033	26.732	55.532	0.297	9.912	0.051	0.412	0.034	0.029	99.001	47.05
020522-53 (100) plag #8-rim	Ollia	6.352	0.049	26.373	56.571	0.374	8.864	0.015	0.32	0.079	0.006	99.003	42.61

Table 5 (cont'd)

Enclave Plagioclase

Sample	Dome	Grain Type	Na_2O	MgO	Al_2O_3	SiO_2	K_2O	CaO	TiO_2
020522-51 (94) enclave plag #1	Bulalo	Needle-like	3.10	0.08	31.41	49.24	0.11	14.42	0.04
020522-51 (94) enclave plag #2	Bulalo	Needle-like	2.90	0.07	31.47	48.94	0.08	14.73	0.03
020522-51tav (96)* plag #1-1	Bulalo	Needle-like	3.38	0.12	31.21	49.68	0.11	13.99	0.04
020522-51tav (96)* plag #1-2	Bulalo	Needle-like	2.75	0.15	31.52	47.78	0.09	15.37	0.01
020522-51tav (96)* plag #2-1	Bulalo	Needle-like	2.71	0.14	31.93	47.67	0.07	15.37	0.04
020522-51tav (96)* plag #2-2	Bulalo	Needle-like	3.32	0.12	30.94	49.67	0.11	13.91	0.05
020522-51tav (96)* plag #4-1	Bulalo	Needle-like	2.56	0.16	32.02	47.83	0.09	15.35	0.01
020522-51 (94) plag #8-core	Bulalo	Phenocryst	2.98	0.09	31.18	48.46	0.09	14.91	0.03
020522-51 (94) plag #8-rim	Bulalo	Phenocryst	5.64	0.03	27.72	54.70	0.30	10.11	-0.02
020522-51 (94)- plag #10-core	Bulalo	Phenocryst	5.79	0.02	26.80	55.11	0.32	9.29	0.01
020522-51 (94) plag #10-rim-a	Bulalo	Phenocryst	6.42	0.04	20.18	64.82	1.66	4.12	0.09
020522-51tav (96)* plag #3-1	Bulalo	Phenocryst	3.56	0.09	30.26	50.20	0.16	13.34	0.02
020522-51tav (96)* plag #3-2	Bulalo	Phenocryst	2.55	0.09	32.27	48.07	0.07	15.64	0.01
020517-2m (31) plag #6	Calamba	Needle-like	2.97	0.03	29.71	47.71	0.19	14.45	0.03
020517-2m (31) plag#5-core	Calamba	Phenocryst	1.12	0.08	34.68	45.16	0.04	18.46	0.02
020517-2m (31) plag #5-rim	Calamba	Phenocryst	3.20	0.10	31.13	49.49	0.20	14.83	0.04
020517-2d (24) enclave plag #1-rim	Calamba	Phenocryst	5.94	0.03	27.10	55.77	0.38	9.67	0.02
020517-2d (24) enclave plag #1-edge	Calamba	Phenocryst	4.54	0.03	29.39	52.49	0.25	12.25	0.02

Table 5 (cont'd)

Sample	BaO	FeO	SrO	Total	% An
020522-51 (94) enclave plag #1	0.68	0.17	0.02	99.27	71.52
020522-51 (94) enclave plag #2	0.59	0.00	0.01	98.82	73.39
020522-51tav (96)* plag #1-1	0.77	0.11	0.02	99.42	69.13
020522-51tav (96)* plag #1-2	0.88	0.00	0.00	98.55	75.16
020522-51tav (96)* plag #2-1	0.80	0.00	0.00	98.72	75.50
020522-51tav (96)* plag #2-2	0.77	0.00	0.00	98.88	69.39
020522-51tav (96)* plag #4-1	0.90	0.00	0.00	98.91	76.41
020522-51 (94) plag #8-core	0.59	0.10	-0.04	98.42	73.07
020522-51 (94) plag #8-rim	0.46	0.12	0.06	99.13	48.92
020522-51 (94)- plag #10-core	0.24	-0.05	-0.10	97.56	46.12
020522-51 (94) plag #10-rim-a	0.39	-0.04	-0.02	97.69	23.25
020522-51tav (96)* plag #3-1	0.75	0.00	0.01	98.39	66.78
020522-51tav (96)* plag #3-2	0.68	0.02	0.01	99.40	76.92
020517-2m (31) plag #6	0.00	0.83	0.00	95.91	72.07
020517-2m (31) plag#5-core	0.00	0.58	0.00	100.12	89.94
020517-2m (31) plag #5-rim	0.00	0.77	0.00	99.75	71.13
020517-2d (24) enclave plag #1-rim	0.00	0.39	0.00	99.30	58.97
020517-2d (24) enclave plag #1-edge	0.02	0.45	0.00	99.45	46.33

Table 5 (cont'd)

Sample	Dome	Grain Type	Na$_2$O	MgO	Al$_2$O$_3$	SiO$_2$	K$_2$O	CaO	TiO$_2$
020522-57/av (105)* plag#3-1	Olila	Needle-like	3.91	0.11	29.57	50.70	0.14	12.97	0.04
020522-57/av (105)* plag#3-2	Olila	Needle-like	4.43	0.09	29.07	52.17	0.19	12.14	0.01
020522-57/av (105)* plag#4-1	Olila	Needle-like	5.84	0.05	27.64	55.87	0.33	9.47	0.02
020522-57/av (105)* plag #4-2	Olila	Needle-like	5.08	0.07	28.49	53.96	0.22	10.69	0.04
020522-53 (100) plag #6-core2	Olila	Phenocryst	5.49	0.05	28.07	55.02	0.27	10.66	0.04
020522-53 (100) plag #6-rim	Olila	Phenocryst	6.65	0.01	25.52	58.01	0.39	8.05	0.02
020522-53 (100) plag #7-core	Olila	Phenocryst	5.54	0.02	27.18	55.01	0.29	9.93	0.02
020522-53 (100) plag #7-rim	Olila	Phenocryst	5.19	0.03	27.69	53.80	0.26	10.93	0.02
020522-53 (100) plag #8-core	Olila	Phenocryst	5.97	0.03	26.73	55.53	0.30	9.91	0.05
020522-53 (100) plag #8-rim	Olila	Phenocryst	6.35	0.05	26.37	56.57	0.37	8.86	0.02
020522-53 (100) enclave plag#1-core	Olila	Phenocryst	5.84	0.03	27.55	55.94	0.31	9.48	0.01
020522-53 (100) enclave plag #1-rim	Olila	Phenocryst	6.15	0.04	26.15	57.10	0.49	8.62	0.01
020522-53 (100) enclave plag #2-core	Olila	Phenocryst	1.80	0.02	33.66	45.98	0.04	16.60	0.01
020522-53 (100) enclave plag#2-rim	Olila	Phenocryst	4.94	0.02	28.50	53.47	0.26	10.95	0.02
020522-57/av (105)* plag#1-core	Olila	Phenocryst	0.97	0.07	34.77	44.49	0.04	18.45	0.00
020522-57/av (105)* plag#1-rim	Olila	Phenocryst	0.97	0.03	34.67	44.56	0.01	18.58	0.00
020522-57/av (105)* plag #2-core	Olila	Phenocryst	0.97	0.05	34.65	44.47	0.02	18.58	0.00
020522-57/av (105)* plag #2-rim	Olila	Phenocryst	0.92	0.06	35.03	43.94	0.03	18.41	0.00

Table 5 (cont'd)

Sample	BaO	FeO	SrO	Total	% An
020522-57/av (105)* plag#3-1	0.92	0.08	0.00	98.43	64.21
020522-57/av (105)* plag#3-2	0.72	0.00	0.00	98.82	59.55
020522-57/av (105)* plag#4-1	0.53	0.14	0.00	99.89	46.35
020522-57/av (105)* plag #4-2	0.62	0.00	0.00	99.17	53.06
020522-53 (100) plag #6-core2	0.42	-0.02	-0.01	99.99	39.21
020522-53 (100) plag #6-rim	0.24	0.09	-0.01	98.97	48.83
020522-53 (100) plag #7-core	0.44	0.09	0.01	98.53	52.95
020522-53 (100) plag #7-rim	0.40	0.11	-0.01	98.43	48.93
020522-53 (100) plag #8-core	0.41	0.03	0.03	99.00	47.05
020522-53 (100) plag #8-rim	0.32	0.08	0.01	99.00	42.61
020522-53 (100) enclave plag#1-core	0.29	0.00	0.06	99.48	46.45
020522-53 (100) enclave plag #1-rim	0.42	0.08	0.10	99.18	42.37
020522-53 (100) enclave plag #2-core	0.62	0.01	0.06	98.78	83.38
020522-53 (100) enclave plag#2-rim	0.39	0.02	0.00	98.59	54.18
020522-57/av (105)* plag#1-core	0.60	0.11	0.00	99.50	91.10
020522-57/av (105)* plag#1-rim	0.66	0.00	0.00	99.50	91.31
020522-57/av (105)* plag #2-core	0.58	0.00	0.03	99.34	91.29
020522-57/av (105)* plag #2-rim	0.69	0.00	0.00	99.08	97.58

Table 6 -Hornblende Analyses*

Sample	Dome	Na$_2$O	MgO	Al$_2$O$_3$	SiO$_2$	Cl	K$_2$O	CaO	TiO$_2$	MnO	FeO	Total	Mg #
020518-2c (15) hbl #2-1	Bijang	1.57	15.57	7.19	45.46	0.11	0.40	11.06	1.62	0.63	11.64	95.40	57.22
020518-2c (15) hbl #2-2	Bijang	1.76	16.00	7.97	46.58	0.07	0.56	11.23	1.74	0.39	11.59	98.15	58.00
020518-2c (15) hbl #3-1	Bijang	1.92	15.06	9.67	45.14	0.10	0.61	11.78	2.18	0.41	12.75	99.75	54.16
020518-2c (15) hbl #3-2	Bijang	1.67	16.36	7.41	46.69	0.07	0.49	11.52	1.83	0.38	11.52	98.08	58.68
020518-2c (15) hbl #4-2	Bijang	1.62	16.61	7.35	47.45	0.05	0.48	11.31	1.72	0.42	11.36	98.47	59.39
020518-2c (15) hbl #4-1	Bijang	1.50	16.83	7.14	47.23	0.09	0.41	11.52	1.33	0.52	11.63	98.30	59.15
020522-51(94)- hbl #1-1	Bulalo	1.84	15.96	7.64	46.90	0.06	0.47	11.30	1.74	0.57	11.62	98.25	57.87
020522-51(94)- hbl #1-2	Bulalo	1.69	16.17	7.22	47.29	0.07	0.48	11.27	1.59	0.57	12.02	98.54	57.35
020522-51(94)- hbl #2-1	Bulalo	2.01	15.23	8.74	45.11	0.08	0.53	11.51	2.12	0.50	11.82	97.87	56.29
020522-51(94)- hbl #2-2	Bulalo	2.07	15.52	8.79	45.53	0.07	0.53	11.57	2.16	0.44	11.98	98.82	56.44
020522-51(94)- hbl #5-1	Bulalo	2.51	14.51	12.31	41.56	0.01	0.41	11.60	2.27	0.17	12.92	98.41	52.90
020522-51(94)- hbl #5-2	Bulalo	2.42	14.33	11.00	43.25	0.03	0.46	11.37	2.08	0.29	12.65	97.97	53.12
020522-51(94)- hbl #6-1	Bulalo	2.40	12.09	13.47	43.34	0.05	0.82	10.96	2.05	0.19	12.07	97.56	50.06
020522-51(94)- hbl #6-2	Bulalo	2.29	13.59	11.61	42.53	0.03	0.53	11.57	1.74	0.36	13.85	98.28	49.53
020522-51 (94) enclave hbl #2-1	Bulalo	2.46	13.94	13.05	41.00	0.03	0.46	11.83	2.14	0.15	12.80	97.97	52.14
020522-51 (94) enclave hbl #2-2	Bulalo	2.36	14.72	11.96	42.40	0.00	0.52	11.80	2.35	0.29	12.25	98.77	54.59
020522-51 (94) enclave hbl #3-1	Bulalo	2.41	14.20	13.45	40.28	0.02	0.55	11.65	2.31	0.16	12.57	97.60	53.06
020522-51 (94) enclave hbl #3-2	Bulalo	1.98	15.22	9.33	44.58	0.07	0.41	10.94	1.59	0.81	13.21	98.23	53.53
020517-2e (16) hbl #1-1	Calamba	2.49	13.39	11.46	41.80	0.04	0.56	11.39	2.11	0.26	14.74	98.46	47.61
020517-2e (16) hbl #1-2	Calamba	2.54	13.78	11.24	42.26	0.03	0.56	11.11	2.52	0.25	14.01	98.46	49.60
020517-2e (16) hbl #2-1	Calamba	2.52	15.09	12.05	42.19	0.02	0.50	11.32	2.51	0.18	12.37	98.90	54.94
020517-2e (16) hbl #2-2	Calamba	2.63	14.16	11.89	42.19	0.04	0.53	11.38	2.58	0.21	13.48	99.77	51.23
020517-2h (16) hbl #3-1 enclave	Calamba	2.65	15.23	12.70	41.72	0.01	0.58	11.75	2.86	0.16	11.33	99.36	57.34
020517-2e (16) hbl #3-2 enclave	Calamba	2.67	15.17	11.22	42.89	0.06	0.48	11.24	2.91	0.28	12.03	99.14	55.78
020522-53 (100)- hbl #1-1	Olila	1.86	15.78	8.39	46.30	0.08	0.46	11.70	2.07	0.47	12.08	99.40	56.64
020522-53 (100)- hbl #1-2	Olila	1.85	15.85	7.73	46.99	0.09	0.47	11.29	1.89	0.59	12.11	99.07	56.70
020522-53 (100)- hbl #3-1	Olila	2.48	15.35	10.73	43.66	0.04	0.45	11.25	2.26	0.32	12.32	99.08	55.47
020522-53 (100)- hbl #3-2	Olila	2.27	14.57	10.55	43.57	0.07	0.57	11.50	2.57	0.40	12.45	98.63	53.94

Table 6 (cont'd)

Sample	Dome	Na$_2$O	MgO	Al$_2$O$_3$	SiO$_2$	Cl	K$_2$O	CaO	TiO$_2$	MnO	FeO	Total	Mg #
020522-53 (100)- hbl #4-1	Olila	2.02	15.60	8.12	46.36	0.08	0.53	11.56	2.29	0.52	11.98	99.13	56.55
020522-53 (100)- hbl #4-2	Olila	2.20	14.68	9.42	44.69	0.06	0.54	11.31	2.02	0.49	12.81	98.38	53.39
020522-53 (100)- hbl #5-1	Olila	1.75	16.11	7.61	47.36	0.08	0.49	11.36	1.66	0.58	11.42	98.52	58.52
020522-53 (100)- hbl #5-2	Olila	1.79	16.13	7.42	47.50	0.09	0.41	11.31	1.66	0.56	11.53	98.55	58.33
020522-53 (100) enclave hbl-#2-1	Olila	2.47	15.36	12.05	41.28	0.02	0.59	11.66	2.62	0.18	11.37	97.70	57.46
020522-53 (100)- hbl #6-1	Olila	2.51	14.24	12.16	41.91	0.00	0.62	11.80	2.74	0.22	11.84	98.20	54.60
020522-53 (100)- hbl #6-2	Olila	1.91	16.13	8.06	46.90	0.07	0.46	11.29	1.97	0.49	11.94	99.45	57.47
020522-53 (100) enclave hbl-#1-1	Olila	2.38	14.77	12.00	41.33	0.03	0.59	11.84	2.74	0.24	12.19	98.19	54.80
020522-53 (100) enclave hbl-#1-2	Olila	1.76	16.13	7.71	46.56	0.06	0.43	11.13	1.89	0.51	11.92	98.25	57.51
020522-53 (100) enclave hbl-#2-2	Olila	2.27	14.14	11.24	42.18	0.05	0.52	11.26	2.27	0.48	13.57	98.00	51.03
020522-53 (100)- hbl #4-2	Olila	2.20	14.68	9.42	44.69	0.06	0.54	11.31	2.02	0.49	12.81	98.38	53.39

* Cr$_2$O$_3$ was also analyzed, all values were <0.05

88

Table 7- Pyroxene Analyses

Orthopyroxene

Sample	Dome	Na$_2$O	MgO	Al$_2$O$_3$	SiO$_2$	Cl	K$_2$O
020518-2c (15) pyx#2-1	Bijang	0.04	25.70	0.76	53.41	0.01	0.03
020518-2c (15) pyx#2-2	Bijang	0.04	25.82	0.63	54.03	0.00	0.03
020518-2c (15) pyx#3-1	Bijang	0.03	26.06	0.70	53.45	0.01	0.04
020518-2c (15) pyx#3-2	Bijang	0.08	26.69	0.48	54.27	0.01	0.03
020518-2c (15) pyx #4-1	Bijang	0.02	25.94	0.72	53.46	0.00	0.01
020518-2c (15) pyx #4-2	Bijang	0.03	25.70	0.70	53.65	0.03	0.00
020518-2c (15) pyx #5-1	Bijang	0.05	25.93	0.72	53.86	0.02	0.03
020518-2c (15) pyx #5-2	Bijang	0.02	26.52	0.50	54.38	0.00	0.01
020522-51 (94) pyx #1-1	Bulalo	0.04	25.06	0.66	52.95	0.00	0.00
020522-51 (94) pyx #1-2	Bulalo	0.02	25.59	0.49	53.51	0.01	0.01
020522-51 (94) pyx #2-1	Bulalo	0.01	24.33	0.48	53.46	0.00	0.02
020522-51 (94) pyx #2-2	Bulalo	0.00	25.17	0.52	53.46	0.00	0.01
020522-51 (94) pyx #3-1	Bulalo	0.02	24.53	0.49	53.31	0.01	0.02
020522-51 (94) pyx #3-2	Bulalo	0.01	25.59	0.55	53.38	0.01	0.01
020522-51 (94) pyx #4-1	Bulalo	0.02	24.96	0.47	53.03	0.00	0.02
020522-51 (94) pyx #4-2	Bulalo	0.03	25.57	0.48	53.66	0.02	0.04
020522-51 (94) pyx #5-1	Bulalo	0.03	25.46	0.70	53.38	0.01	0.00
020522-51 (94) pyx #5-2	Bulalo	0.03	25.43	0.51	53.48	0.01	0.02
020522-53 (100)- unk #1- pyx	Olila	0.03	24.37	0.66	53.71	0.00	0.02
020522-53 (100)- unk #2- pyx	Olila	0.03	25.64	0.64	54.09	0.02	0.00
020522-53 (100) pyx #4-1	Olila	0.01	24.82	0.98	52.45	0.00	0.00
020522-53 (100) pyx #4-2	Olila	0.01	25.57	0.59	53.65	0.01	0.01
020522-53 (100) pyx #7-1	Olila	0.01	24.57	0.44	53.56	0.00	0.00
020522-53 (100) pyx #7-2	Olila	0.03	24.73	0.46	53.77	0.01	0.00
020522-53 (100) pyx #8-1	Olila	0.02	24.61	0.60	53.15	0.00	0.02
020522-53 (100) pyx #8-2	Olila	0.01	25.70	0.46	53.73	0.00	0.02
020522-53 (100) pyx #11-1	Olila	0.02	24.25	0.98	52.83	0.01	0.01

Table 7 (cont'd)

Sample	CaO	TiO_2	Cr_2O_3	MnO	FeO	Total	Mg#	% En
020518-2c (15) pyx#2-1	0.71	0.13	0.00	1.57	18.85	101.23	57.69	69.87
020518-2c (15) pyx#2-2	0.77	0.10	0.00	1.40	18.08	100.91	58.82	70.71
020518-2c (15) pyx#3-1	0.78	0.13	0.02	1.56	18.68	101.46	58.24	70.24
020518-2c (15) pyx#3-2	0.78	0.09	0.00	1.38	18.42	102.23	59.16	71.01
020518-2c (15) pyx #4-1	0.84	0.12	0.00	1.66	18.78	101.55	58.01	69.96
020518-2c (15) pyx #4-2	0.67	0.11	0.01	1.58	18.81	101.33	57.74	69.97
020518-2c (15) pyx #5-1	1.02	0.17	0.11	1.44	18.70	102.06	58.10	69.79
020518-2c (15) pyx #5-2	0.90	0.13	0.00	1.31	18.47	102.33	58.96	70.67
020522-51 (94) pyx #1-1	0.89	0.11	0.00	1.77	19.17	100.64	56.65	68.75
020522-51 (94) pyx #1-2	0.67	0.12	0.00	1.80	18.90	101.17	57.52	69.79
020522-51 (94) pyx #2-1	1.07	0.13	0.02	2.26	19.42	101.21	55.61	67.60
020522-51 (94) pyx #2-2	0.63	0.06	0.00	1.90	18.80	100.56	57.24	69.58
020522-51 (94) pyx #3-1	0.76	0.11	0.01	2.21	19.69	101.20	55.47	67.90
020522-51 (94) pyx #3-2	0.75	0.09	0.00	1.76	18.70	100.89	57.78	69.89
020522-51 (94) pyx #4-1	0.67	0.09	0.00	2.03	19.50	100.77	56.13	68.61
020522-51 (94) pyx #4-2	0.62	0.07	0.02	1.89	18.87	101.27	57.54	69.87
020522-51 (94) pyx #5-1	0.79	0.18	0.03	1.51	18.58	100.66	57.82	69.85
020522-51 (94) pyx #5-2	0.82	0.13	0.00	1.61	18.64	100.70	57.71	69.72
020522-53 (100)- unk #1- pyx	0.99	0.15	0.01	2.03	18.84	100.80	56.41	68.37
020522-53 (100)- unk #2- pyx	0.96	0.11	0.01	1.51	18.86	101.86	57.62	69.48
020522-53 (100) pyx #4-1	0.77	0.18	0.00	2.11	19.32	100.71	56.22	68.54
020522-53 (100) pyx #4-2	0.99	0.15	0.00	1.66	18.61	101.24	57.88	69.64
020522-53 (100) pyx #7-1	0.67	0.13	0.00	2.21	19.06	100.65	56.31	68.74
020522-53 (100) pyx #7-2	0.68	0.11	0.00	1.98	19.09	100.91	56.43	68.83
020522-53 (100) pyx #8-1	0.71	0.11	0.00	2.13	18.91	100.26	56.55	68.89
020522-53 (100) pyx #8-2	0.72	0.14	0.00	1.57	18.37	100.73	58.31	70.36
020522-53 (100) pyx #11-1	0.78	0.19	0.00	2.10	19.00	100.19	56.07	68.38

Table 7 (cont'd)

Sample	Dome	Na$_2$O	MgO	Al$_2$O$_3$	SiO$_2$	Cl	K$_2$O
020522-53 (100) pyx #11-2	Olila	0.01	25.22	0.52	53.33	0.00	0.0042
020517-2h (16) pyx #5-1	Calamba	0.03	25.20	0.85	54.20	0.01	0
020517-2h (16) pyx #5-2	Calamba	0.04	25.08	0.71	53.64	0.02	0
020517-2h (16) pyx #6-1	Calamba	0.03	23.30	0.69	51.48	0.00	0.0046
020517-2h (16) pyx #6-2	Calamba	0.02	25.28	1.03	53.47	0.02	0.0105
020517-2h (16) pyx #7-1	Calamba	0.03	24.16	0.53	52.24	0.00	0
020517-2h (16) pyx #7-2	Calamba	0.02	24.19	0.54	51.73	0.00	0.0042
020517-2h (16) pyx #10-1	Calamba	0.02	25.60	0.58	53.68	0.01	0.0153
020517-2h (16) pyx #10-2	Calamba	0.03	23.92	0.48	51.66	0.00	0.0071
020517-2h (16) pyx #11	Calamba	0.02	24.14	0.90	52.31	0.00	0.0071

Clinopyroxene

Sample	Dome	Na$_2$O	MgO	Al$_2$O$_3$	SiO$_2$	Cl	K$_2$O
020517-2h (16) pyx #1-1	Calamba	0.42	15.60	1.58	52.57	0.01	0.025
020517-2h (16) pyx #1-2	Calamba	0.39	15.76	1.39	52.48	0.02	0.034
020517-2h (16) pyx #2-1	Calamba	0.42	15.56	1.18	52.74	0.02	0.025
020517-2h (16) pyx #2-2	Calamba	0.39	15.52	1.47	52.77	0.02	0
020517-2h (16) pyx #3-1	Calamba	0.36	14.84	1.29	51.31	0.01	0
020517-2h (16) pyx #3-2	Calamba	0.36	15.75	1.32	52.80	0.02	0.004
020517-2e (16) pyx #4-1	Calamba	0.40	16.03	1.94	52.22	0.00	0
020517-2h (16) pyx #9-1	Calamba	0.24	17.48	2.25	52.89	0.01	0.031
020517-2h (16) pyx #12-1	Calamba	0.35	15.30	1.12	51.46	0.01	0.001
020517-2h (16) pyx #12-2	Calamba	0.39	15.11	1.17	51.21	0.00	0
020517-2d (24) pyx #6-2	Calamba	0.40	15.65	1.37	52.24	0.00	0.0036
020517-2d (24) pyx #7-1	Calamba	0.35	15.37	1.35	52.22	0.00	0.0086
020517-2d (24) pyx #7-2	Calamba	0.31	15.83	1.33	52.20	0.00	0.0034

Table 7 (cont'd)

Sample	CaO	TiO_2	Cr_2O_3	MnO	FeO	Total	Mg #	% En
020522-53 (100) pyx #11-2	0.75	0.14	0.00	2.07	19.24	101.30	56.73	69.00
020517-2h (16) pyx #5-1	1.23	0.25	0.00	0.88	19.50	102.15	56.38	68.07
020517-2h (16) pyx #5-2	1.06	0.19	0.00	0.82	19.63	101.20	56.09	68.06
020517-2h (16) pyx #6-1	2.60	0.17	0.00	0.85	17.17	96.30	57.58	66.97
020517-2h (16) pyx #6-2	1.26	0.25	0.00	0.92	17.63	99.91	58.91	70.07
020517-2h (16) pyx #7-1	1.03	0.15	0.00	1.04	17.51	96.69	57.98	69.58
020517-2h (16) pyx #7-2	1.10	0.16	0.03	1.05	17.15	95.99	58.52	69.91
020517-2h (16) pyx #10-1	1.12	0.15	0.04	1.11	17.26	99.58	59.73	70.94
020517-2h (16) pyx #10-2	1.09	0.17	0.00	1.13	17.19	95.74	58.18	69.64
020517-2h (16) pyx #11	1.17	0.18	0.00	0.87	17.13	96.73	58.50	69.79

Clinopyroxene

Sample	CaO	TiO_2	Cr_2O_3	MnO	FeO	Total	Mg #	% En
020517-2h (16) pyx #1-1	21.81	0.37	0.04	0.50	8.89	101.82	63.68	43.02
020517-2h (16) pyx #1-2	21.62	0.42	0.02	0.51	8.56	101.19	64.80	43.65
020517-2h (16) pyx #2-1	21.54	0.33	0.00	0.58	8.82	101.22	63.81	43.23
020517-2h (16) pyx #2-2	21.78	0.33	0.00	0.52	8.56	101.36	64.45	43.15
020517-2h (16) pyx #3-1	20.83	0.35	0.02	0.46	8.23	97.69	64.31	43.10
020517-2h (16) pyx #3-2	21.73	0.33	0.02	0.50	8.35	101.18	65.34	43.68
020517-2e (16) pyx #4-1	20.52	0.56	0.03	0.61	9.68	101.99	62.35	44.27
020517-2h (16) pyx #9-1	16.26	0.31	0.00	0.36	7.83	97.72	69.07	52.10
020517-2h (16) pyx #12-1	19.49	0.30	0.02	0.58	7.72	96.34	66.46	45.49
020517-2h (16) pyx #12-2	19.51	0.32	0.00	0.49	7.82	96.04	65.90	45.08
020517-2d (24) pyx #6-2	20.91	0.37	0.00	0.52	8.93	100.41	63.67	43.86
020517-2d (24) pyx #7-1	20.90	0.37	0.03	0.47	8.29	99.42	64.97	43.87
020517-2d (24) pyx #7-2	20.82	0.40	0.00	0.58	8.62	100.14	64.75	44.43

Table 8- Fe-Ti Oxide Analyses

Ilmenite

Sample	Dome	MgO	Al₂O₃	SiO₂	CaO	TiO₂	V₂O₃	Cr₂O₃	MnO	FeO	Total
020517-2h (16) il #1	Calamba	0.98	0.07	0.13	0.01	43.83	0.29	0.06	0.84	51.86	98.08
020517-2d (24) il #1	Calamba	2.81	0.32	0.05	0.02	39.52	0.30	0.03	0.59	52.19	95.83

Magnetite

Sample	Dome	MgO	Al₂O₃	SiO₂	CaO	TiO₂	V₂O₃	Cr₂O₃	MnO	FeO	Total
020518-2c (15) mag #1	Bijang	1.93	1.95	0.15	0.02	6.33	0.34	0.00	0.70	81.78	93.20
020518-2c (15) mag #2	Bijang	1.78	1.96	0.09	0.01	6.44	0.44	0.00	0.70	82.69	94.09
020518-2c (15) mag #3	Bijang	1.92	2.06	0.13	0.03	6.26	0.38	0.00	0.71	82.66	94.13
020518-2c (15) mag #4	Bijang	1.88	1.96	0.07	0.03	5.60	0.32	0.23	0.79	83.14	94.02
020518-2c (15) mag #5	Bijang	1.77	1.97	0.09	0.03	6.60	0.44	0.00	0.70	83.07	94.67
020518-2c (15) mag #6-1	Bijang	1.82	1.97	0.07	0.05	6.25	0.44	0.11	0.76	83.02	94.48
020518-2c (15) mag #6-2	Bijang	1.90	1.98	0.07	0.00	5.93	0.41	0.00	0.76	82.86	93.91
020518-2c (15) unk #1 (mag)	Bijang	1.75	1.98	0.11	0.05	5.27	0.30	0.00	0.72	83.42	93.60
020522-51(94) mag #1-1	Bulalo	1.57	1.75	0.09	0.08	6.46	0.35	0.06	0.91	83.52	94.77
020522-51(94) mag #1-2	Bulalo	1.45	1.83	0.12	0.03	6.26	0.39	0.00	0.92	83.33	94.34
020522-51(94) mag #2	Bulalo	1.67	1.78	0.11	0.01	6.30	0.38	0.04	0.83	83.31	94.43
020522-51(94) mag #3	Bulalo	1.54	1.79	0.12	0.01	6.29	0.32	0.05	0.84	83.25	94.21
020522-51(94) mag #4	Bulalo	1.55	1.71	0.10	0.01	6.27	0.37	0.01	0.82	83.25	94.09
020522-51(94) mag #5	Bulalo	1.56	1.82	0.12	0.01	5.96	0.31	0.01	0.84	83.13	93.75
020522-51 (94) enclave mag #1	Bulalo	1.52	1.71	0.13	0.06	6.11	0.47	0.15	0.98	83.26	94.38
020522-51 (94) enclave mag #2	Bulalo	1.36	1.60	0.10	0.06	6.08	0.48	0.07	0.99	83.49	94.22
020517-2h (16) mag #1-1	Calamba	1.45	2.40	0.46	0.02	9.81	0.43	0.03	0.64	79.75	94.98
020517-2h (16) mag #1-2	Calamba	1.49	2.34	0.35	0.02	9.63	0.47	0.03	0.64	80.03	95.00
020517-2h (16) mag #1-3	Calamba	1.40	2.47	0.38	0.01	10.44	0.57	0.06	0.49	78.06	93.87
020517-2h (16) mag #2	Calamba	0.54	1.76	0.48	0.00	9.41	0.52	0.04	0.71	81.16	94.62
020517-2h (16) mag #3	Calamba	0.77	2.17	0.17	0.00	11.42	0.40	0.03	0.67	80.57	96.21

Table 8 cont.

Sample	Dome	MgO	Al_2O_3	SiO_2	CaO	TiO_2	V_2O_3	Cr_2O_3	MnO	FeO	Total
020517-2h (16) mag #4	Calamba	0.80	2.25	0.17	0.03	10.01	0.51	0.07	0.68	81.12	95.65
020517-2h (16) mag #5	Calamba	0.52	1.96	0.23	0.00	9.88	0.54	0.03	0.74	81.58	95.48
020522-53 (100) mag #1	Olila	1.86	2.06	0.11	0.06	6.71	0.37	0.03	0.78	82.54	94.52
020522-53 (100) mag #2	Olila	1.95	2.07	0.11	0.02	6.67	0.40	0.02	0.74	83.31	95.26
020522-53 (100) mag #3	Olila	2.00	2.19	0.12	0.10	6.37	0.41	0.03	0.80	82.45	94.47
020522-53 (100) mag #4	Olila	1.78	2.04	0.09	0.01	6.94	0.39	0.03	0.75	82.97	95.00
020522-53 (100) mag #5	Olila	1.81	2.11	0.08	0.00	6.80	0.44	0.01	0.76	81.96	93.98
020522-53 (100) mag #6	Olila	1.74	2.12	0.25	0.01	5.89	0.31	0.03	0.73	82.48	93.55

Table 9a- Trace Elements- Plagioclase

sample	Dome	Ba	Sr	CaO	Sr/Ba	%An
020518-1c (15) plag #2-core	Bijang	454.76	1107.77	8.07	2.44	38.65
020518-1c (15) plag #2-mid1	Bijang	483.71	1172.92	8.22	2.42	39.19
020518-1c (15) plag #2-mid2	Bijang	700.15	1198.92	7.80	1.71	37.65
020518-1c (15) plag #2-edge	Bijang	559.65	1080.12	8.00	1.93	38.14
020518-1c (15) plag #4-core	Bijang	216.32	755.79	10.08	3.49	47.48
020518-1c (15) plag#4-mid	Bijang	382.48	714.68	7.21	1.87	34.41
020522-51 (94) plag #2-core	Bulalo	192.33	1166.58	11.16	6.07	55.27
020522-51 (94) plag #2-rim	Bulalo	634.50	1455.11	10.47	2.29	51.82
020522-51 (94) plag #4-core	Bulalo	282.31	1122.49	9.98	3.98	47.88
020522-51 (94) plag #6 core-a	Bulalo	327.45	1343.83	9.58	4.10	46.02
020522-51 (94) plag #6-mid	Bulalo	366.27	971.77	7.00	2.65	33.76
020522-51 (94) plag #6-rim	Bulalo	519.38	967.63	7.01	1.86	33.81
020517-2d (24) plag #1-core	Calamba	296.64	965.87	9.32	3.26	44.56
020517-2d (24) plag #1-rim	Calamba	298.99	841.89	8.39	2.82	40.37
020517-2d (24) plag #3-core	Calamba	267.32	1657.04	16.81	6.20	82.94
020517-2d (24) plag #3-mid	Calamba	237.63	1136.34	12.12	4.78	59.15
020517-2d (24) plag #3-rim	Calamba	372.01	899.07	8.32	2.42	40.42
020517-2d (24) plag #5-core	Calamba	233.14	1024.65	10.18	4.39	49.08
020517-2d (24) plag #5-mid	Calamba	340.56	973.69	8.67	2.86	41.80
020517-2m (31) plag #1-core	Calamba	320.65	1046.02	9.73	3.26	46.66
020517-2m (31) plag#1-mid	Calamba	255.34	944.20	9.17	3.70	43.66
020517-2m (31) plag#1-rim	Calamba	392.80	1019.35	9.27	2.60	44.51
020517-2m (31) plag#3-core	Calamba	205.49	1261.65	13.36	6.14	64.41
020517-2m (31) plag #3-mid1	Calamba	270.20	1069.61	9.60	3.96	46.68
020517-2m (31) plag #3-mid2	Calamba	488.70	1167.35	10.10	2.39	48.79
020517-2m (31) plag #3-rim	Calamba	388.68	960.22	8.92	2.47	42.63
020517-2m (31) plag #4-core	Calamba	350.01	823.11	8.85	2.35	42.97
020517-2m (31) plag #4-mid	Calamba	400.30	958.72	8.56	2.39	41.07
020517-2m (31) plag #4-rim	Calamba	351.92	905.17	8.91	2.57	43.06

Table 9b- Trace Elements- Enclave Plagioclase

sample	Dome	Ba	Sr	CaO	Sr/Ba	%An
020522-51 (94) plag #8-core	Bulalo	181.27	1192.05	14.91	6.58	73.07
020522-51 (94) plag #10-core	Bulalo	142.74	880.49	9.29	6.17	46.12
020522-51 (94) plag #10-mid	Bulalo	490.34	1012.58	7.03	2.07	34.39
020522-53 (100) plag #6-core	Olila	574.66	2230.81	10.66	3.88	50.98
020522-53 (100) plag #8-core	Olila	378.23	1567.02	9.91	4.14	47.05

REFERENCES CITED

Andersen, D.J., Lindsley, D.H. and Davidson, P.M., 1993, QUILF: A PASCAL program to assess equilibria among Fe-Mg-Mn-Ti oxides, pyroxenes, olivine, and quartz, Computers and Geosciences, 19, 9: 1333-1350

Aquino, D.J.P, 2004, Surface Structure Analysis for the Bulalo Geothermal Field: Possible Implications to Local and Regional Tectonics, MS thesis, University of the Philippines: 116 pp.

Bates, R.L. and Jackson, J.A. (eds), 1957, Dictionary of Geological Terms, American Geological Institute, New York: 571 pp.

Bautista, B.C., Bautista, M.L.P., Oike, K., Wu, F.T. and Punongbuyan, R.S., 2001, A new insight on the geometry of the subduction slabs in northern Luzon, Philippines, Tectonophysics, 339: 279-310

Beard, J.S. and Lofgren, G.E., 1991, Dehydration melting and water-saturated melting of basaltic and andesitic greenstones and amphibolites at 1, 3, 6 and 9 kbar, Journal of Petrology, 32: 365-401

Bindeman, I.N. and Valley, J.W., 2003, Rapid generation of both high- and low-$\delta^{18}O$, large volume silicic magmas at the Timber Mountain/Oasis Valley caldera complex, Nevada, GSA Bulletin, 115, 5: 581-595

Blundy, J.D. and Wood, B.J., 1991, Crystal-chemical controls on the partitioning of Sr and Ba between plagioclase feldspar, silicate melts, and hydrothermal solutions, Geochimica Acta Cosmochimica, 55: 193-209

Brophy, J.G., and Dreher, S.T., 2000, The origin and composition gaps at South Sister volcano, central Oregon: implications for fractional crystallization processes beneath active calc-alkaline volcanoes, Journal of Volcanology and Geothermal Research, 102: 287-307

Browne, B.L., Eichelberger, J.C., Patino, L.C., Vogel, T.A., Uto, K. and Hoshizumi, H., 2004, Magma mingling as indicated by texture and geochemistry of plagioclase phenocrysts from Unzen Volcano, SW Japan, Journal of Volcanology and Geophysical Research, in review

Cardwell, R.K., Isacks, B.L. and Karig, D.E., 1980, The spatial distribution of earthquakes, focal mechanism solutions and subducted lithosphere in the Philippine and Northeastern Indonesian Islands, in Hayes, D.E. (ed), The Tectonic and Geologic Evolution of Southeast Asian Seas and Islands, Geophysical Monograph 23: 1-35

Catane, S.G. and Arpa, C.B., 1998, Large-scale eruptions of Laguna caldera: contributions to the accretion and other geomorphic developments of Metro Manila and adjacent provinces. PHIVOLCS internal report.

Clayton, R.N., Goldsmith, J.R. and Mayeda, T.K., 1989, Oxygen isotope fractionation in quartz, albite, anorthite, and calcite, Geochimica Acta Cosmochimica 53, 3: 725-733

Cruz, J.B., 1992, Petrology and geochemistry of lavas from the Makiling-Banahaw volcanic complex, Southern Luzon, Philippines, M.S. thesis, University of Illinois, Chicago, IL

Defant, M.J., Jacques, D., Maury, R.C., Boer, J.D. and Joron, J-L., 1989, Geochemistry and tectonic setting of the Luzon Arc, Philippines, Geological Society of America Bulletin, 101: 663-672

Gertisser, R. and Keller, J, 2000, From basalt to dacite: origin and evolution of the calc-alkaline series of Salina, Aeolian Arc, Italy, Contributions to Mineralogy and Petrology, 139: 607-626

Ginibre, C., Worner, G. and Kronz, A., 2002, Minor- and trace-element zoning in plagioclase: implications for magma chamber processes at Parinacota volcano, northern Chile, Contributions to Mineralogy and Petrology, 143: 300-315

Grove, T.L., Elkins-Tanton, L.T., Parman, S.W., Chatterjee, N., Muntener, O. and Gaetani, G.A., 2003, Fractional crystallization and mantle melting controls on calc-alkaline differentiation trends, Contriubtions to Mineralogy and Petrology, 145: 515-533

Hannah, R.S., Vogel, T.A., Patino, L.C., Alvarado, G.E., Perez, W. and Smith, D.R., 2002, Origin of silicic volcanic rocks in Central Costa Rica: a study of a chemically variable ash-flow sheet in the Tiribi Tuff, Bulletin of Volcanology, 64: 117-133

Heizler, M., 2003, $^{40}Ar/^{39}Ar$ geochronology results for volcanic rocks from the Philippines, Internal report NMGRL-IR-302&341 prepared for the New Mexico Geochronological Laboratory

Knittel, U., Defant, M.J. and Raczek, I., 1988, Recent enrichment in the source region of arc magmas from Luzon island Philippines: Sr and Nd isotopic evidence, Geology, 16: 73-76

LeBas, M.J., LeMaitre, R.W., Streckeisen, A., and Zanettin, B., 1986, A chemical classification of volcanic rocks based on the total alkali silica diagram, Journal of Petrology, 27: 745-750.

Mukasa, S.B., Flower, M.F.J. and Miklius, 1994, The Nd-, Sr- and Pb-isotopic character of lavas from Taal, Laguna de Bay and Arayat volcanoes, southwestern Luzon, Philippines: Implications for arc magma petrogenesis, Tectonophysics, 235: 205-221

Muntener, O., Kelemen, P.B and Grove, T.L., 2001, The role of H_2O during crystallization of primitive arc magmas under uppermost mantle conditions and genesis of igneous pyroxenites: an experimental study, Contributions to Mineralogy and Petrology, 141, 6: 643-658

Oles, D., 1991, Geology of the Macolod Corridor intersecting the Bataan-Mindoro island arc, The Philippines, Final report for German Research Society Project No. Fo53/16-1 to 2 and German Agency for Technical Cooperation Project No. 85.2522.2-06.100

Price, R.C., Stewart, R.B., Woodhead, J.D. and Smith, I.E.M., 1999, Petrogenesis of high-K arc magmas: Evidence from Egmont Volcano, North Island, New Zealand, Journal of Petrology, 40, 1: 167-197

Riley, T.R., Leat, P.T., Pankhurst, R.J. and Harris, C., 2001, Origins of large volume rhyolitic volcanism in the Antarctic Peninsula and Patagonia by crustal melting, Journal of Petrology, 40, 1: 1043-4065

Rollinson, H., 1993, Using geochemical data: evaluation, presentation interpretation, Longman Group, UK: 352 pp.

Singer, B.S., Myers, J.D. and Frost, C.D., 1992, Mid-Pleistocene lavas from the Seguam volcanic center, central Aleutian arc: closed system fractional crystallization of a basalt to rhyodacite eruptive suite, Contributions to Mineralogy and Petrology, 42, 6: 1043-1065

Singer, B.S., Dungan, M.A. and Layne, G.D., 1995, Textures and Sr, Ba, Mg, Fe, K, and Ti compositional profiles in volcanic plagioclase: Clues to the dynamics of calc-alkaline magma chambers, American Mineralogist, 80: 776-798

Smith, I.E.M., Stewart, R.B. and Price, R.C., 2003a, The petrology of large intra-oceanic eruption: the Sandy Bay Tephra, Kermadec Arc Southwest Pacific, Journal of Volcanology and Geothermal Research, 124: 173-194

Smith, I.E.M., Worthington, T.J., Stewart, R.B., Price, R.C. and Gamble, J.A., 2003b, Felsic Volcanism in the Kermadec arc, SW Pacific: crustal recycling in an oceanic setting, in Larter, R.D. and Leat, P.T., (eds), Intra-Oceanic Subduction

Systems: Tectonic and Magmatic Processes, Geological Society of London Special Publications, 219: 99-118

Snyder, D. and Tait, S., 1998, The imprint of basalt on the geochemistry of silicic magmas, Earth and Planetary Science Letters, 160, 3-4: 433-445

Sudo, M., Listanco, E.L., Ishikawa, N., Tagami, T., Kamata, H. and Tatsumi, Y., 2001, K-Ar dating of the volcanic rocks from the Macolod Corridor in Southwestern Luzon, Philippines: Toward an understanding of the Quaternary volcanism and tectonics, Journal of the Geological Society of the Philippines, 55, 1-2: 89-104

Sun, S. and McDonough, W.F., 1989, Chemical and isotopic systematics of oceanic basalts: implications for mantle compositions and processes in Saunders, A.D. and Norry, M.J. (eds), Magmatism in the Ocean Basins, Geological Society Special Publication No. 42: 313-345

Tamura, Y and Tatsumi, Y, 2002, Remelting of an andesitic crust as a possible origin for rhyolitic magma in oceanic arcs: an example from the Izu-Bonin Arc, Journal of Petrology, 43, 6: 1029-1047

Tamura, Y., Yuhara, M., Ishii, T., Irino, N. and Shukuno, H., 2003, Andesites and Dacites from Daisen Volcano, Japan: Partial-to-total remelting of an andesite magma body, Journal of Petrology, 44, 12: 2243-2260

Tepley III, F.J., Davidson, J.P. and Clynne, M.A., 1999, Magmatic interactions as recorded in plagioclase phenocrysts of Chaos Crags, Lassen Volcanic Center, California, Journal of Petrology, 40, 5: 787-806

Watts, R.B., de Silva, S.L. and de Rios, G.J., 1999, Effusive eruption of viscous silicic magma triggered and driven by recharge: a case study of the Cerro Chascon-Runtu Jarita Dome Complex in Southwest Bolivia, Bulletin of Volcanology, 60: 241-264

Viray, E., 2003, Origin and evolution of the Nicaraguan silicic ash-flow sheets, M.S. Thesis, Michigan State University, East Lansing, MI